

# Testing dynamical torsion effects on the charged black hole's shadow, deflection angle and greybody with M87\* and Sgr A\* from EHT

Reggie C. Pantig<sup>1,\*</sup> and Ali Övgün<sup>2,†</sup>

<sup>1</sup>*Physics Department, De La Salle University, 2401 Taft Avenue, Manila, 1004 Philippines*

<sup>2</sup>*Physics Department, Eastern Mediterranean University,  
Famagusta, 99628 North Cyprus via Mersin 10, Turkey.*

(Dated: June 7, 2022)

Poincare Gauge's theory of gravity is the most noteworthy alternative extension of general relativity that has a correspondence between spin and spacetime geometry. In this paper, we used Reissner-Nordstrom-de Sitter and anti-de Sitter solutions, where torsion  $\tau$  is added as an independent field, to analyze the weak deflection angles  $\hat{\alpha}$  of massive and null particles in finite distance regime. We then applied  $\hat{\alpha}$  to determine the Einstein ring formation in M87\* and Sgr. A\* and determine that relative to Earth's location from these black holes, massive torsion effects can provide considerable deviation, while the cosmological constant's effect remains negligible. Furthermore, we also explored how the torsion parameter affects the shadow radius perceived by both static and co-moving (with cosmic expansion) observers in a Universe dominated by dark energy, matter, and radiation. Our findings indicate that torsion and cosmological constant parameters affect the shadow radius differently between observers in static and co-moving states. We have also shown how the torsion parameter affects the luminosity of the photonsphere by studying the shadow with infalling accretion. The calculation of the quasinormal modes, greybody bounds, and high-energy absorption cross-section was also affected by the torsion parameter considerably.

PACS numbers: 95.30.Sf, 04.70.-s, 97.60.Lf, 04.50.+h

Keywords: Black hole; Deflection angle; Shadow; Thin accretion disk; Torsion; Quasinormal modes; Greybody factor

## I. INTRODUCTION

Einstein's theory of General Relativity (GR) is the most successful theory of gravity which has passed the test of time [1]. After Einstein had shown that light should be bent by gravity in GR, Sir Arthur Eddington tested this assumption at the 1919 Total Eclipse of the Sun [2]. GR also predicts the most important compact object there is - black holes (BHs) whose features not only fascinated theoretical physicists, but also those in the field of experimental physics. Recently, the "chirp" due to the gravitational field produced by the coalescence of two BHs is observed in LIGO/VIRGO collaboration [3] and shadow images of the BHs at the center of M87 and Milky Way galaxies are captured by the Event Horizon Telescope (EHT) [4, 5].

The correspondence between the geometry of the spacetime with the energy-momentum of the matter is one of the most fascinating foundations of GR. Energy-momentum tensor is the source of the gravitational field and can be written in terms of the curvature tensor. To extend the GR, one can consider the intrinsic angular momentum of matter as an alternative source of the interactions. The gauge approach in field theory has been studied by early works of Weyl [6], Cartan [7], Fock [8], and later by Utiyama [9], Sciama [10], and Kibble [11]. For more details, one can check the review paper on the development of gauge gravity based on the Poincare symmetry group [12] which is one of the extensions of the GR known as Poincare Gauge theory of gravity (PGTG). PGTG has an

asymmetric affine connection that stands within a Riemann-Cartan manifold (combine the curvature with torsion) which provides a well-defined correspondence between spin and the geometry of spacetime [13]. In this theory, the source of the torsion is a non-trivial spin density tensor. Recently, Cembranos and Valcarcel have found a new exact solution charged black hole solution with massive torsion in a PGTG containing higher-order corrections quadratic in the curvature tensor [14]. In this paper, we aim to explore the torsion effects in combination with the cosmological constant. To our knowledge, very few studies were carried out concerning BHs with a torsion parameter. The torsion effects on black holes can have different physical interpretations depending on how it was derived from the Einstein field equation. For example, in Ref. [15], the torsion charge's effect on the black hole shadow was studied and explored. Torsion effects are also important to information [16]. Long-ranged limit due to the black hole in torsion bigravity was also considered [17]. When it comes to the cosmological constant parameter  $\Lambda$ , a well-known black hole spacetime that incorporates the de Sitter spacetime ( $+\Lambda$ ) is called the Kottler metric [18]. Driven by the cosmological constant, the black hole shadow with such an influence was studied in [19, 20]. Different treatment can also be found in Ref. [21]. Recently, the formalism that involves  $\Lambda$  to the shadow perceived by a co-moving observer was applied in McVittie spacetime [22]. Interestingly, it allowed the examination of the approximate angular radius of the shadow under the effect of which type of Universe we live in (dark energy, matter, or radiation-dominated). The effect of the cosmological constant under different field theories was also considered by other authors (See Ref. [23]). We observe in these papers that they lack the anti-de Sitter analysis, and we aim in this paper to provide an exploration of it.

\* reggie.pantig@dlsu.edu.ph

† ali.ovgun@emu.edu.tr

The black hole shadow is so important in the study of BH physics since it can tell us the mass and size of the BH, how the spacetime is distorted near it, and how matter and radiation falls near the event horizon - a region of no escape. It was Synge in 1966 who first theoretically studied the shadow of the simplest solution to the Einstein field equation - the Schwarzschild metric [24], and in 1979, Lunin et al. gave the corresponding expression for the angular radius of the shadow [25]. Since then, the formalism was applied to a number of static and spherically symmetric black hole spacetime models to explore how certain parameters induce deviations from the known black hole shadow size [26–71]. Pantig et al. [72, 73] have studied the possible effects of dark matter on a Schwarzschild black hole with the correction of extended uncertainty principle on black hole shadow and also effect of dark matter on the weak deflection angle by black holes at the galactic center. Övgün has showed [74] that a confining charge gives a significant contribution to the shadow of the black hole with confining electric potential in scalar-tensor description of regularized 4-dimensional Einstein-Gauss-Bonnet gravity. Okyay and Övgün have studied the nonlinear electrodynamics effects on the black hole shadow [75]. The black hole shadow in symmergent gravity has been investigated in [76]. Moreover, Pantig and Övgün have studied the effect of Dehnen dark matter halo profile on a black hole in an ultra-faint dwarf galaxy [77]. Slowly rotating Kerr-like black hole in bumblebee gravity has been studied by Kuang and Övgün in [78]. Authors provide some constraint on parameters of NLE using the observations of M87\* and Sgr. A\* from EHT [79]. Övgün et al. have showed the shadow cast and deflection angle of Kerr-Newman-Kasuya spacetime [80], and also [81] studied the shadow of black hole in Einstein-Cartan-Kibble-Sciama theory of gravity.

Gravitational lensing is a powerful tool to test gravity [82–86]. There are several commonly used calculation methods of gravitational lensing and the most used method for the investigation of the deflection angle in weak field limits is the one proposed by Gibbons and Werner as an alternative method for the asymptotically flat black holes [87]. First, they obtained the optical metric of the black hole spacetime and then applied the Gauss-Bonnet theorem (GBT). Then, Werner extended it for stationary spacetimes and calculated the deflection angle of the Kerr black hole in weak fields [88]. Nowadays, there are many applications of this method on black holes, wormholes and other spacetimes [89–106]. In the framework of dynamical torsion, our one of the aim is to investigate the effect of dynamical torsion on the weak deflection angle of both massive and null particles by applying the Gauss-bonnet theorem.

Here is how the paper is organized: In Sect. II we introduce the metric of the black hole with massive torsion. In Sect. III, we study how the torsion parameter affects the deflection angle both for massive and null particles. Sect. IV–V is dedicated to the analysis of the null geodesic and shadow cast for static and co-moving observers. The shadow with infalling spherical accretion is explored in Sect. VI. The eikonal (geometric optics) limit of quasinormal modes will be analyzed in Sect. VII. We also explored the greybody factors and high energy absorption cross-section using the Sinc approximation in Sect.

VIII. We formulate our conclusion in Sect. IX and state future research directions. Throughout the paper, we will use the natural units  $G = c = 1$  and the signature  $(-, +, +, +)$ .

## II. BLACK HOLES IN QUADRATIC POINCARÉ GAUGE GRAVITY MODEL WITH MASSIVE TORSION

Classical solutions of the Poincaré gauge help us to better understand the influence of torsion on the gravitational dynamics. In this section, we focus our attention on the static and spherically symmetric solution found by Cembranos and Valcarcel [14], in which the electric charge of the standard RN metric is imitated by a torsion-induced parameter  $\kappa$ .

The general gravitational action related to original Poincaré gauge model and incorporate the three independent quadratic scalar invariants of torsion into this expression, which represent the mass terms of the mentioned quantity [14]:

$$S = \frac{1}{16\pi} \int d^4x \sqrt{-g} \left[ \mathcal{L}_m - \tilde{R} - \frac{1}{4} (d_1 + d_2) \tilde{R}^2 - \frac{1}{4} (d_1 + d_2 + 4c_1 + 2c_2) \tilde{R}_{\lambda\rho\mu\nu} \tilde{R}^{\mu\nu\lambda\rho} + c_1 \tilde{R}_{\lambda\rho\mu\nu} \tilde{R}^{\lambda\rho\mu\nu} + c_2 \tilde{R}_{\lambda\rho\mu\nu} \tilde{R}^{\lambda\mu\rho\nu} + d_1 \tilde{R}_{\mu\nu} \tilde{R}^{\mu\nu} + d_2 \tilde{R}_{\mu\nu} \tilde{R}^{\nu\mu} + \alpha T_{\lambda\mu\nu} T^{\lambda\mu\nu} + \beta T_{\lambda\mu\nu} T^{\mu\lambda\nu} + \gamma T^\lambda_{\lambda\nu} T^\mu_{\mu} \right], \quad (1)$$

where  $c_1, c_2, d_1, d_2, \alpha, \beta$  and  $\gamma$  are constant parameters. In this paper, we focus our attention on the static and spherically symmetric solution found by Cembranos and Valcarcel [14], in which the electric charge of the standard RN metric is imitated by a massive torsion-induced parameter in quadratic Poincaré gauge gravity model as follows:

$$ds^2 = -f(r)^2 dt^2 + \frac{dr^2}{f(r)^2} + r^2 (d\theta^2 + \sin^2 \theta d\varphi^2), \quad (2)$$

where the metric function reads

$$f(r) = 1 - \frac{2m}{r} + \frac{\tau^2 + Q^2}{r^2} - \frac{\Lambda r^2}{3}, \quad (3)$$

where, for simplicity, we let the constant parameter  $d_1$  to be absorbed by the torsion parameter  $\kappa$  and write  $\tau = \sqrt{d_1} \kappa$ . In addition, we wrote the combined effect of the electric and magnetic charges as  $Q^2 = q_e^2 + q_m^2$ . As one will also notice, the metric is generalized to include the cosmological constant.

The outer horizon is located at the larger root of  $f(r) = 0$  and this can be visualized through Fig. 1. We can also see in the figure how the dS and AdS case are different in terms of null boundary formation. Continuing, one can calculate the following 4-velocity via

$$u = u^t \partial_t, \quad (4)$$

and then normalization condition is satisfied by

$$1 = u^\mu u_\mu \quad (5)$$

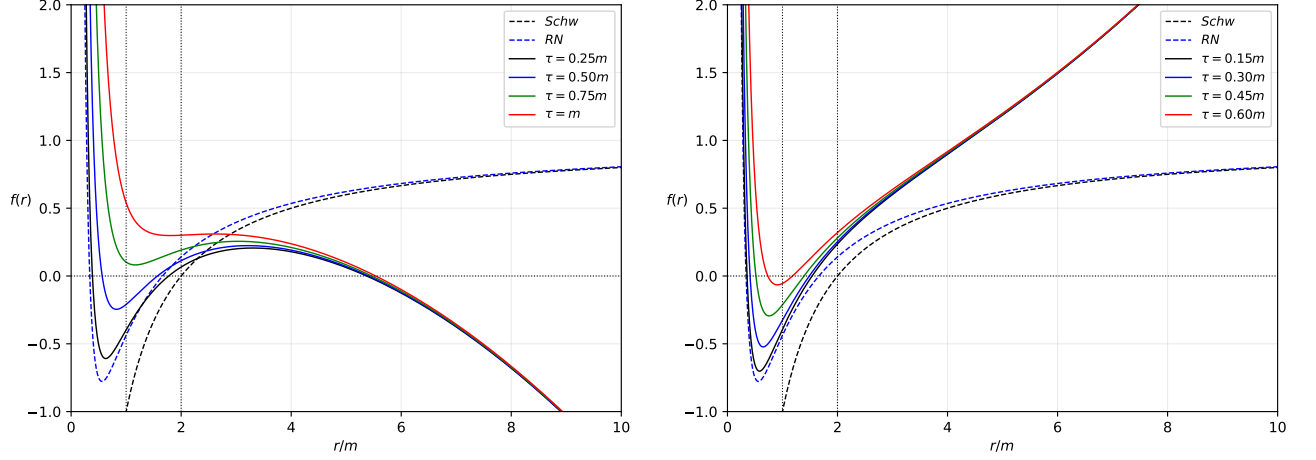


FIG. 1. The lapse function  $f(r)$  behavior in response to different values of the torsion parameter  $\tau$ . Here, we take  $m = 1$ ,  $Q = 0.75m$ , and scaled the cosmological constant to  $\Lambda = 0.0675 \text{ m}^{-2}$ . The left and right figures corresponds to de Sitter (dS) case  $+\Lambda$ , and anti-de Sitter (AdS) case  $-\Lambda$  respectively.

where  $u^t = \frac{1}{\sqrt{g_{tt}}}$ . Since the metric components are functions of  $r$  and  $\theta$ , particle acceleration  $a^\mu$  is obtained from

$$a^\mu = -g^{\mu\nu} \partial_\nu \ln u^t.$$

Surface gravity ( $\kappa$ ) is defined as follows

$$dl_{\text{prop}} = \lim_{r \rightarrow r_h} \frac{\sqrt{a^\mu a_\mu}}{u^t}$$

Hence, the surface gravity is obtained as follows to find black hole temperature:

$$\kappa := \frac{1}{2} \partial_r f^2 \Big|_{r_+}, \quad T := \frac{\kappa}{2\pi}. \quad (6)$$

Then, a simple calculation of the horizon area yields

$$A_{\text{BH}} = \int_0^{2\pi} d\varphi \int_0^\pi \sqrt{-g} d\theta = 4\pi r_h. \quad (7)$$

Hence, the entropy of black hole becomes

$$S_{\text{BH}} = \frac{A_{\text{BH}}}{4} = \pi r_h. \quad (8)$$

### III. WEAK DEFLECTION ANGLE USING GAUSS-BONNET THEOREM

In this section we present the calculation of the deflection angle of a massive particle around a charged black hole with dynamical torsion and cosmological constant. For a static, spherically symmetric (SSS) spacetime,

$$\begin{aligned} ds^2 &= g_{\mu\nu} dx^\mu dx^\nu \\ &= -A(r) dt^2 + B(r) dr^2 + C(r) d\Omega^2 \end{aligned} \quad (9)$$

the Jacobi metric reads

$$\begin{aligned} dl^2 &= g_{ij} dx^i dx^j \\ &= (E^2 - m^2 A(r)) \left( \frac{B(r)}{A(r)} dr^2 + \frac{C(r)}{A(r)} d\Omega^2 \right), \end{aligned} \quad (10)$$

where  $d\Omega^2 = d\theta^2 + r^2 \sin^2 \theta$  is the line element of the unit two-spheres, and  $E$  is the energy of the massive particle defined by

$$E = \frac{\mu}{\sqrt{1 - v^2}}, \quad (11)$$

where  $v$  is the particle's velocity. In the equatorial plane then where  $\theta = \pi/2$ , the Jacobi metric is reduced to

$$dl^2 = (E^2 - \mu^2 A(r)) \left( \frac{B(r)}{A(r)} dr^2 + \frac{C(r)}{A(r)} d\phi^2 \right) \quad (12)$$

without loss of generality. The determinant of the Jacobi metric above can also be easily calculated as

$$g = \frac{B(r)C(r)}{A(r)^2} (E^2 - \mu^2 A(r))^2. \quad (13)$$

Next, we will use these equations to find the weak deflection angle using the Gauss-Bonnet theorem (GBT), originally stated as

$$\iint_D K dS + \sum_{a=1}^N \int_{\partial D_a} \kappa_g dl + \sum_{a=1}^N \theta_a = 2\pi \chi(D). \quad (14)$$

Here, the Gaussian curvature  $K$  describing the domain  $D$  is a freely orientable  $2D$  curved surface  $S$  with infinitesimal area element is  $dS$ . The boundary of  $D$  are given by  $\partial D_a$  ( $a=1, 2, \dots, N$ ), and the geodesic curvature  $\kappa_g$  is integrated over the path  $dl$  along a positive convention. Also,  $\theta_a$  is the jump

angle, which  $\chi(D)$  is the Euler characteristic where in our case is equal to 1 since  $D$  is in a non-singular region.

It was shown by [105] that in a SSS spacetime with no asymptotic flatness, Eq. (14) can be written as

$$\hat{\alpha} = \iint_{\square_{r_{\text{co}}}^R \square_{r_{\text{co}}}^S} K dS + \phi_{\text{RS}}, \quad (15)$$

where  $r_{\text{co}}$  is the radius of the particle's circular orbit, and S and R are the radial positions of the source and receiver respectively. These are the integration domains, and we note that the infinitesimal curve surface  $dS$  is given by

$$dS = \sqrt{g} dr d\phi. \quad (16)$$

Furthermore,  $\phi_{\text{RS}}$  is the coordinate position angle between the source and the receiver defined as  $\phi_{\text{RS}} = \phi_{\text{R}} - \phi_{\text{S}}$ , which can be found through the iterative solution of

$$\begin{aligned} F(u) &= \left( \frac{du}{d\phi} \right)^2 \\ &= \frac{C(u)^2 u^4}{A(u)B(u)} \left[ \left( \frac{E}{J} \right)^2 - A(u) \left( \frac{1}{J^2} + \frac{1}{C(u)} \right) \right], \end{aligned} \quad (17)$$

where we have used the substitution  $r = 1/u$  and the angular momentum of the massive particle

$$J = \frac{\mu v b}{\sqrt{1 - v^2}}, \quad (18)$$

where  $b$  is the impact parameter. With Eq. (2), we find

$$\begin{aligned} F(u) &= \frac{E^2 - 1}{J^2} - u^2 - u^2 \left( \frac{1}{J^2} + u^2 \right) (\tau^2 + Q^2) \\ &+ \left( \frac{1}{J^2 u^2} + 1 \right) \frac{\Lambda}{3} + \left( \frac{1}{J^2} + u^2 \right) 2mu. \end{aligned} \quad (19)$$

Doing the iteration method, we find

$$u(\phi) = \frac{\sin(\phi)}{b} + \frac{1 + v^2 \cos^2(\phi)}{b^2 v^2} m - \frac{(\tau^2 + Q^2)}{2v^2 b^3} + \frac{\Lambda b}{6v^2}. \quad (20)$$

In terms of affine connections, the Gaussian curvature  $K$  is defined as

$$\begin{aligned} K &= \frac{1}{\sqrt{g}} \left[ \frac{\partial}{\partial \phi} \left( \frac{\sqrt{g}}{g_{rr}} \Gamma_{rr}^\phi \right) - \frac{\partial}{\partial r} \left( \frac{\sqrt{g}}{g_{rr}} \Gamma_{r\phi}^\phi \right) \right] \\ &= -\frac{1}{\sqrt{g}} \left[ \frac{\partial}{\partial r} \left( \frac{\sqrt{g}}{g_{rr}} \Gamma_{r\phi}^\phi \right) \right] \end{aligned} \quad (21)$$

since  $\Gamma_{rr}^\phi = 0$  for Eq. (12). If in a certain spacetime there is an analytical solution for the  $r_{\text{co}}$ , then we have the relation

$$\int_{r_{\text{co}}}^{r(\phi)} K \sqrt{g} dr = - \frac{A(r) (E^2 - A(r)) C' - E^2 C(r) A(r)'}{2A(r) (E^2 - A(r)) \sqrt{B(r)C(r)}} \Big|_{r=r(\phi)} - \frac{(\tau^2 + Q^2)u}{\sqrt{2}\sqrt{bv^2(1-b^2u^2)}} + \frac{b^3 u \Lambda}{6\sqrt{2}v^2\sqrt{1-b^2u^2}} \quad (22)$$

since

$$\left[ \int K \sqrt{g} dr \right] \Big|_{r=r_{\text{co}}} = 0. \quad (23)$$

The prime denotes differentiation with respect to  $r$ . The weak deflection angle for non-asymptotic spacetime is then [105],

$$\hat{\alpha} = \int_{\phi_{\text{S}}}^{\phi_{\text{R}}} \left[ - \frac{A(r) (E^2 - A(r)) C' - E^2 C(r) A(r)'}{2A(r) (E^2 - A(r)) \sqrt{B(r)C(r)}} \Big|_{r=r(\phi)} \right] \times d\phi + \phi_{\text{RS}}. \quad (24)$$

Using Eq. (20) in Eq. (22), we find

$$\begin{aligned} \left[ \int K \sqrt{g} dr \right] \Big|_{r=r(\phi)} &= - \frac{(2E^2 - 1) m (\cos(\phi_{\text{R}}) - \cos(\phi_{\text{S}}))}{(E^2 - 1) b} \\ &- \frac{(3E^2 - 1) ((\tau^2 + Q^2)) \left[ \phi_{\text{RS}} - \frac{(\sin(2\phi_{\text{R}}) - \sin(2\phi_{\text{S}}))}{2} \right]}{4(E^2 - 1) b^2} \\ &+ \frac{(1 + E^2) b^2 \Lambda (\cot(\phi_{\text{R}}) - \cot(\phi_{\text{S}}))}{6(E^2 - 1)} - \phi_{\text{RS}} \\ &+ \mathcal{O}[m(\tau^2 + Q^2), m\Lambda, \Lambda(\tau^2 + Q^2), m(\tau^2 + Q^2)\Lambda], \end{aligned} \quad (25)$$

where we retained  $E$  to avoid the clutter caused by the velocity  $v$ , and chosen only the dominant terms. To find the expression for  $\phi$ , we use Eq. (20) and solve it. For the source and receiver respectively, we find

$$\begin{aligned} \phi_{\text{S}} &= \arcsin(bu) + \frac{m [v^2 (b^2 u^2 - 1) - 1]}{bv^2 \sqrt{1 - b^2 u^2}} \\ &+ \frac{(\tau^2 + Q^2)}{2b^2 v^2 \sqrt{1 - b^2 u^2}} - \frac{b^2 \Lambda}{3\sqrt{2}v^2 \sqrt{2 - 2b^2 u^2}} \\ &+ \mathcal{O}[m(\tau^2 + Q^2), m\Lambda, \Lambda(\tau^2 + Q^2), m(\tau^2 + Q^2)\Lambda], \end{aligned} \quad (26)$$

$$\begin{aligned} \phi_{\text{R}} &= \pi - \arcsin(bu) - \frac{m [v^2 (b^2 u^2 - 1) - 1]}{bv^2 \sqrt{1 - b^2 u^2}} \\ &- \frac{(\tau^2 + Q^2)}{2b^2 v^2 \sqrt{1 - b^2 u^2}} + \frac{b^2 \Lambda}{3\sqrt{2}v^2 \sqrt{2 - 2b^2 u^2}} \\ &+ \mathcal{O}[m(\tau^2 + Q^2), m\Lambda, \Lambda(\tau^2 + Q^2), m(\tau^2 + Q^2)\Lambda]. \end{aligned} \quad (27)$$

Based on this, we write  $\phi_{\text{RS}} = \pi - 2\phi_{\text{S}}$ . Now, we take note of the following relations:

$$\begin{aligned} \cos(\pi - \phi_{\text{S}}) &= -\cos(\phi_{\text{S}}), \\ \cot(\pi - \phi_{\text{S}}) &= -\cot(\phi_{\text{S}}), \\ \sin(\pi - \phi_{\text{S}}) &= \sin(\phi_{\text{S}}). \end{aligned} \quad (28)$$

The last property makes the sine terms in Eq. (25) to cancel. We find  $\cos(\phi_{\text{S}})$  as

$$\begin{aligned} \cos(\phi_{\text{S}}) &= \sqrt{1 - b^2 u^2} - \frac{mu [v^2 (b^2 u^2 - 1) - 1]}{\sqrt{v^2 (1 - b^2 u^2)}} \\ &- \frac{(\tau^2 + Q^2)u}{\sqrt{2}\sqrt{bv^2(1-b^2u^2)}} + \frac{b^3 u \Lambda}{6\sqrt{2}v^2\sqrt{1-b^2u^2}} \end{aligned}$$

$$+ \mathcal{O}[m(\tau^2 + Q^2), m\Lambda, \Lambda(\tau^2 + Q^2), m(\tau^2 + Q^2)\Lambda], \quad (29)$$

and  $\cot(\phi_S)$  as

$$\begin{aligned} \cot(\phi_S) &= \frac{\sqrt{1-b^2u^2}}{bu} + \frac{m[v^2(-b^2u^2+1)+1]}{b^3u^2v^2\sqrt{1-b^2u^2}} \\ &- \frac{(\tau^2+Q^2)}{2b^4u^2v^2\sqrt{1-b^2u^2}} + \frac{\Lambda}{6\sqrt{2}u^2v^2\sqrt{1-b^2u^2}} \\ &+ \mathcal{O}[m(\tau^2+Q^2), m\Lambda, \Lambda(\tau^2+Q^2), m(\tau^2+Q^2)\Lambda]. \quad (30) \end{aligned}$$

By plugging Eqs. (26)-(30) in Eq. (24), we finally obtain (after also using Eq. (11))

$$\begin{aligned} \hat{\alpha} &\sim \frac{m(v^2+1)}{bv^2} \left( \sqrt{1-b^2u_R^2} + \sqrt{1-b^2u_S^2} \right) \\ &- \frac{(\tau^2+Q^2)(v^2+2)}{4b^2v^2} [\pi - (\arcsin(bu_R) + \arcsin(bu_S))] \\ &+ \frac{b\Lambda(v^2-2)}{6v^2} \left( \frac{\sqrt{1-b^2u_R^2}}{u_R} + \frac{\sqrt{1-b^2u_S^2}}{u_S} \right) \\ &+ \mathcal{O}[m(\tau^2+Q^2), m\Lambda, \Lambda(\tau^2+Q^2), m(\tau^2+Q^2)\Lambda], \quad (31) \end{aligned}$$

which also involves the finite distance  $u_S$  and  $u_R$ . We can approximate this form by making  $u$  to be nearly zero and in such a case,  $b^2u^2 \sim 0$  and we have

$$\begin{aligned} \hat{\alpha} &\sim \frac{2m(v^2+1)}{bv^2} - \frac{(\tau^2+Q^2)\pi(v^2+2)}{4b^2v^2} \\ &+ \frac{b\Lambda(v^2-2)}{6v^2} \left( \frac{1}{u_R} + \frac{1}{u_S} \right) \\ &+ \mathcal{O}[m(\tau^2+Q^2), m\Lambda, \Lambda(\tau^2+Q^2), m(\tau^2+Q^2)\Lambda]. \quad (32) \end{aligned}$$

Note also that for the case of null particles, where  $v = 1$ , the above reduces to a known expression:

$$\begin{aligned} \hat{\alpha} &\sim \frac{4m}{b} - \frac{3\pi(\tau^2+Q^2)}{4b^2} - \frac{b\Lambda}{6} \left( \frac{1}{u_R} + \frac{1}{u_S} \right) \\ &+ \mathcal{O}[m(\tau^2+Q^2), m\Lambda, \Lambda(\tau^2+Q^2), m(\tau^2+Q^2)\Lambda]. \quad (33) \end{aligned}$$

The above is in agreement with the result in Ref. [107]. In Figs. 2 and 3, we plotted the behavior of the weak deflection angle calculated by an observer near the black hole ( $u = 0.5b^{-1}$ ) and far from the black hole  $u = 0.01b^{-1}$ . In each figure, the weak deflection angle of massive and null particles are also compared. We included the locations critical impact parameters to easily identify the allowed values  $\hat{\alpha}$ . Let us start first with similar observations present in these plots. One can see the effect of the increasing value of the torsion parameter decreases the value of  $\hat{\alpha}$ . Also, the change due to the torsion parameter's influence diminishes as the impact parameter  $b/m$  increases, as the cosmological constant dominates large distances. Let us now compare the effect of  $+\Lambda$  between near and remote receivers. First, we can notice that massive particles are more sensitive to the effect of  $\Lambda$  since its deflection angle tends to zero first at large  $b/m$  than the null particles. For remote observer, if  $\Lambda = 0.005 \text{ m}^{-2}$ , it does not produce any  $+\hat{\alpha}$ , hence we lowered the scaled effect to  $\Lambda = 0.0001 \text{ m}^{-2}$ .

It indicates that  $\hat{\alpha}$  itself becomes sensitive  $\Lambda$  as we observe black holes at remote distances. Next is the AdS type that in general, we have the same observation with the dS type in terms of black hole's distance of the receiver. The only key difference is that the  $\hat{\alpha}$  do not approach zero as  $b/m \rightarrow \infty$ .

One observable that involves the weak deflection angle is the Einstein ring, which is very useful for astronomical observations. Let  $D_S$  and  $D_R$  be the position of the source and receiver respectively. The thin lens approximation implies that  $D_{RS} = D_S + D_R$ , and the position of the weak field images is given by

$$D_{RS} \tan \beta = \frac{D_R \sin \theta - D_S \sin(\hat{\alpha} - \theta)}{\cos(\hat{\alpha} - \theta)}. \quad (34)$$

When  $\beta = 0$ , an Einstein ring is formed, and the above equation can be simplified into

$$\theta_E \sim \frac{D_S}{D_{RS}} \hat{\alpha}. \quad (35)$$

Finally, we can use the relation  $b = d_R \sin \theta \sim d_R \theta$  and obtain

$$\begin{aligned} \theta_E &= \frac{-9\pi\epsilon D_R D_S}{4D_R(\Lambda+6)(D_{RS})} \\ &+ \frac{\sqrt{3}D_R D_S \{128(\Lambda+6)(D_{RS})m + 27\pi^2 D_R D_S \epsilon^2\}^{1/2}}{4D_R(\Lambda+6)(D_{RS})} \quad (36) \end{aligned}$$

where the parameter  $\epsilon = (\tau^2 + Q^2)/b^2$ . We plot Eq. (36) in Fig. 4, where it represents a source and a receiver that is close to the black hole. The immediate effect of the torsion parameter is to further decrease the value of the angular radius of the Einstein ring, in comparison to the RN case. The effect is magnified for lower values of  $b/m$  but diminishes as  $b/m$  increases. We could also see the effect of the cosmological constant, where the deviation is very small (see inset plot). If  $\Lambda$  is negative, the dashed red line will only be lower than the solid red line.

Next, let us plot the Einstein ring due to black hole Sgr. A\* and M87\*. See Fig. 5. For Sgr. A\*, we used  $m_{\text{Sgr. A}^*} = 4.3 \times 10^6 M_\odot$  and  $D_R = 8.33 \text{ kpc}$ , and for M87\*,  $m_{\text{M87}^*} = 6.5 \times 10^9 M_\odot$  and  $D_R = 16.8 \text{ Mpc}$ . Note that when  $\tau = 0$ ,  $Q = 0$ , and  $\Lambda = 0$ ,  $\theta_E^{\text{Sgr. A}^*} = 1.453 \mu\text{as}$ , and  $\theta_E^{\text{M87}^*} = 1.257 \mu\text{as}$ . First, we see a differing behavior of the Einstein ring from Fig. 4 because of the vast distance of Earth from these black holes. Moreover, using the actual value of the cosmological constant, its effect is vanishingly small in these cases. Nonetheless, we can see the effect of the torsion parameter on the behavior of the Einstein ring's angular radius. That is, as  $\tau$  increases,  $\theta_E$  decreases. The effect seems to be large, again, at smaller values of  $b/m$  compared to the large values. It then gives the possibility of detecting the effect of torsion, even if  $Q$  is small.

#### IV. NULL GEODESICS AND SHADOWS CAST

We compute for the radius of the photon sphere following the method presented in Perlick et al. [108]. Without loss

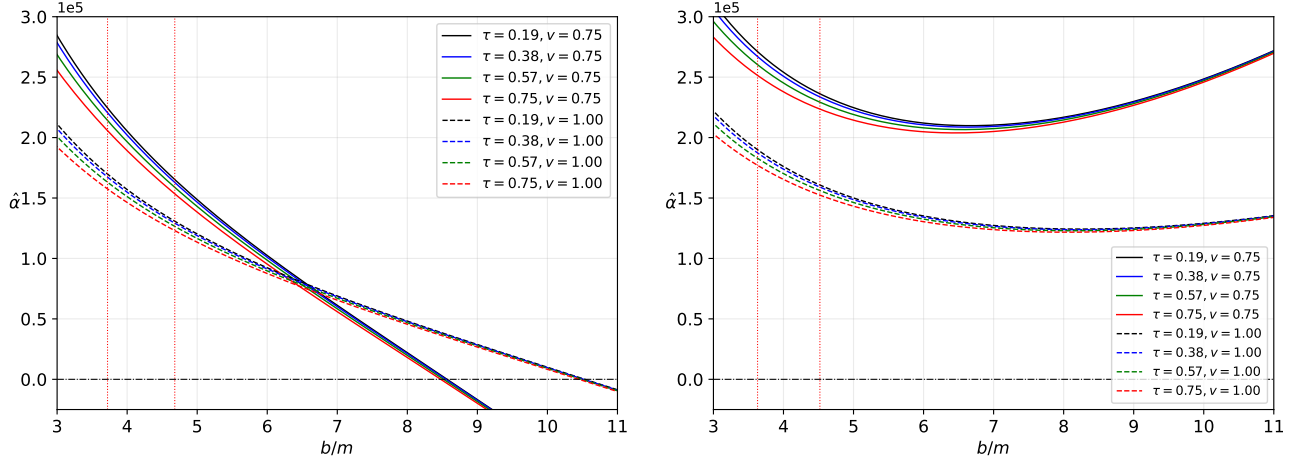


FIG. 2. Comparison of weak deflection angle (Eq. (31)) between a massive particles (solid lines) and null particles (dashed line) as the torsion parameter changes. The left and right vertical dotted red lines are the critical impact parameters for  $\tau = 0.19m$  and  $\tau = 0.75m$  respectively. Finite distance of the source and receiver are considered where it is assumed that  $u_S = u_R = u$  and  $u = 0.5b^{-1}$ . Also in this plot (left),  $Q = 0.75m$ , and  $\Lambda = 0.005 \text{ m}^{-2}$ . The right figure is for  $-\Lambda$ .

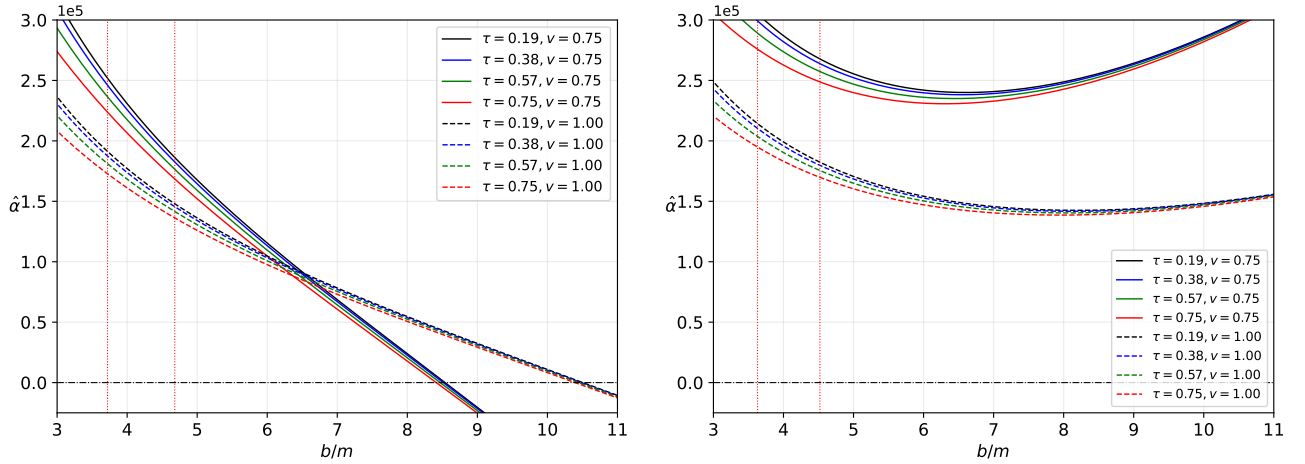


FIG. 3. Comparison of weak deflection angle (Eq. (32)) between massive particles (solid lines) and null particles (dashed line) as the torsion parameter changes. The left and right vertical dotted red lines are the critical impact parameters for  $\tau = 0.19m$  and  $\tau = 0.75m$  respectively. Finite distance of the source and receiver are considered where it is assumed that  $u_S = u_R = u$  and  $u = 0.01b^{-1}$ . Also in this plot (left),  $Q = 0.75m$ , and  $\Lambda = 0.0001 \text{ m}^{-2}$ . The right figure is for  $-\Lambda$ .

of generality, we analyze the null geodesic in the equatorial plane only such that  $\theta = \pi/2$ . For our metric, this means  $D(r) = C(r)$  For a spherically static and symmetric (SSS) spacetime, the Hamiltonian for light rays is in general given by

$$H = \frac{1}{2} g^{ik} p_i p_k = \frac{1}{2} \left( -\frac{p_t^2}{A(r)} + \frac{p_r^2}{B(r)} + \frac{p_\phi^2}{C(r)} \right). \quad (37)$$

The equations of motion for null particles are then

$$\dot{x}^i = \frac{\partial H}{\partial p_i}, \quad \dot{p}_i = -\frac{\partial H}{\partial x^i}. \quad (38)$$

Here,  $\dot{x} = dx/d\lambda$  and  $\dot{p}$  represents the conjugate momenta. Eq. (38) gives

$$\dot{t} = -\frac{p_t}{A(r)}, \quad \dot{\phi} = \frac{p_\phi}{C(r)}, \quad \dot{r} = -\frac{p_r}{B(r)}, \quad (39)$$

and

$$\dot{p}_t = 0, \quad \dot{p}_\phi = 0$$

$$\dot{p}_r = \frac{1}{2} \left( -\frac{p_t^2 A'(r)}{A(r)^2} + \frac{p_r^2 B'(r)}{B(r)^2} + \frac{p_\phi^2 D'(r)}{C(r)} \right). \quad (40)$$

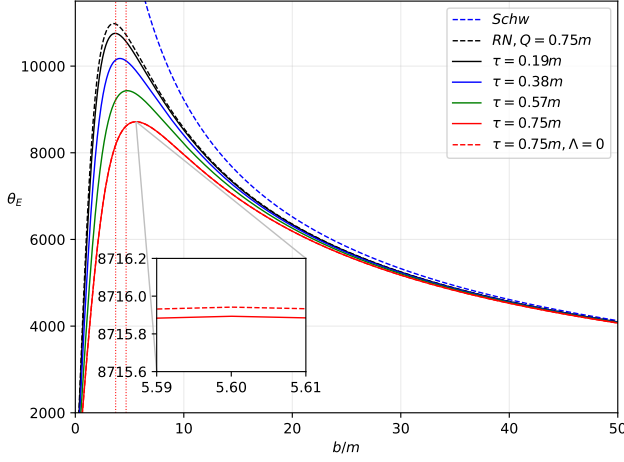


FIG. 4. Plot (theoretical) of the Einstein ring formation in  $\mu\text{as}$ . Here, we set  $Q = 0.75m$ ,  $\Lambda = 0.0001 \text{ m}^{-2}$ , and  $D_S = D_R = 100b$ . The left and right vertical dotted red lines are the critical impact parameters for  $\tau = 0.19m$  and  $\tau = 0.75m$  respectively.

The first line in Eq. (40) implies the existence of the two conserved quantities for null geodesic given as

$$E = A(r) \frac{dt}{d\lambda}, \quad L = C(r) \frac{d\phi}{d\lambda}, \quad (41)$$

where  $\lambda$  is the affine parameter along the light ray. The impact parameter, which is a constant of motion, is then defined as

$$b \equiv \frac{L}{E} = \frac{C(r)}{A(r)} \frac{d\phi}{dt}. \quad (42)$$

Using  $ds = 0$  and Eq. (42), we can obtain the orbit equation as

$$\left( \frac{dr}{d\phi} \right)^2 = \frac{C(r)}{B(r)} \left( \frac{h(r)^2}{b^2} - 1 \right), \quad (43)$$

where  $h(r)^2$  is defined as [108]

$$h(r)^2 = \frac{C(r)}{A(r)}, \quad (44)$$

which is useful because the radius of the photonsphere can be immediately calculated as

$$\frac{d}{dr} \left( \frac{C(r)}{A(r)} \right) = 0, \quad (45)$$

then for our case we have

$$r_{\text{ph}} = \frac{3m}{2} \pm \frac{1}{2} \sqrt{9m^2 - 8(\tau^2 + Q^2)}. \quad (46)$$

In Fig. 6, we plot the location of the photonsphere radius using the exact form in Eq. (46). We can see how the location of the photonsphere varies for different values of  $Q$ . In other words, these are only the allowed values for  $r_{\text{ph}}$  for a given value of

$Q$ . We observe that the effect of increasing torsion parameter value is to decrease the photonsphere radius.

For the black hole shadow, we consider first the static observer. The shadow depends on the initial direction of light rays that spiral towards the outermost photon sphere. We aim to calculate its radius. With careful inspection of the line element, the definition [19]

$$\tan(\alpha_{\text{sh}}) = \lim_{\Delta x \rightarrow 0} \frac{\Delta y}{\Delta x} = \left( \frac{C(r)}{B(r)} \right)^{1/2} \frac{d\phi}{dr} \Big|_{r=r_o}, \quad (47)$$

or

$$\cot^2(\alpha_{\text{sh}}) = \left( \frac{B(r)}{C(r)} \right) \left( \frac{dr}{d\phi} \right)^2 \Big|_{r=r_o}. \quad (48)$$

With the help of Eq. (43) and with simple trigonometry, we then find

$$\sin^2(\alpha_{\text{sh}}) = \frac{b_{\text{crit}}^2}{h(r_o)^2}, \quad (49)$$

where  $b_{\text{crit}}$  is associated with the photonsphere radius. It can be derived by satisfying the condition  $dr/d\phi = 0$  and imposing  $r \rightarrow r_{\text{ph}}$ :

$$b_{\text{crit}}^2 = \frac{h(r)}{[B'(r)C(r) - B(r)C'(r)]} \left[ h(r)B'(r)C(r) - h(r)B(r)C'(r) - 2h'(r)B(r)C(r) \right], \quad (50)$$

where in our case yields

$$b_{\text{crit}}^2 = \frac{6r_{\text{ph}}^3}{3r_{\text{ph}} - 3m - 2\Lambda r_{\text{ph}}^3}. \quad (51)$$

Using the above equation and Eq. (49), we obtain the exact formula for the shadow radius:

$$\mathcal{R}_{\text{sh}} = r_{\text{ph}} \left[ \frac{2 \left( 1 - \frac{2m}{r_o} + \frac{q^2}{r_o^2} - \frac{\Lambda}{3} r_o^2 \right)}{1 - \frac{m}{r_{\text{ph}}} - \frac{2\Lambda}{3} r_{\text{ph}}^2} \right]^{1/2}. \quad (52)$$

Although the photonsphere radius is independent of  $\Lambda$ 's influence, the shadow radius is not. The main reason for this is that the shadow radius is affected by the astrophysical environment induced by  $\Lambda$  as the photons travels toward the observer. Let us first discuss the observational constraint of the torsion parameter using the obtained data from M87\* [4] and Sgr. A\* [5]. For M87\*, the shadow angular diameter is  $\theta_{\text{M87}^*} = 42 \pm 3 \mu\text{as}$ , and the distance of the M87\* from the Earth is  $D = 16.8 \text{ Mpc}$ , and the mass of the M87\* is  $m_{\text{M87}^*} = 6.5 \pm 0.90 \times 10^9 M_{\odot}$ . For Sgr. A\* the shadow angular diameter is  $\theta_{\text{Sgr. A}^*} = 48.7 \pm 7 \mu\text{as}$  (EHT), the distance of the Sgr. A\* from the Earth is  $D = 8277 \pm 33 \text{ pc}$  and mass of the black hole is  $m_{\text{Sgr. A}^*} = 4.3 \pm 0.013 \times 10^6 M_{\odot}$  (VLTI). Let us now calculate the diameter of the shadow size in units of the black hole mass using

$$d_{\text{sh}} = \frac{D\theta}{M}. \quad (53)$$

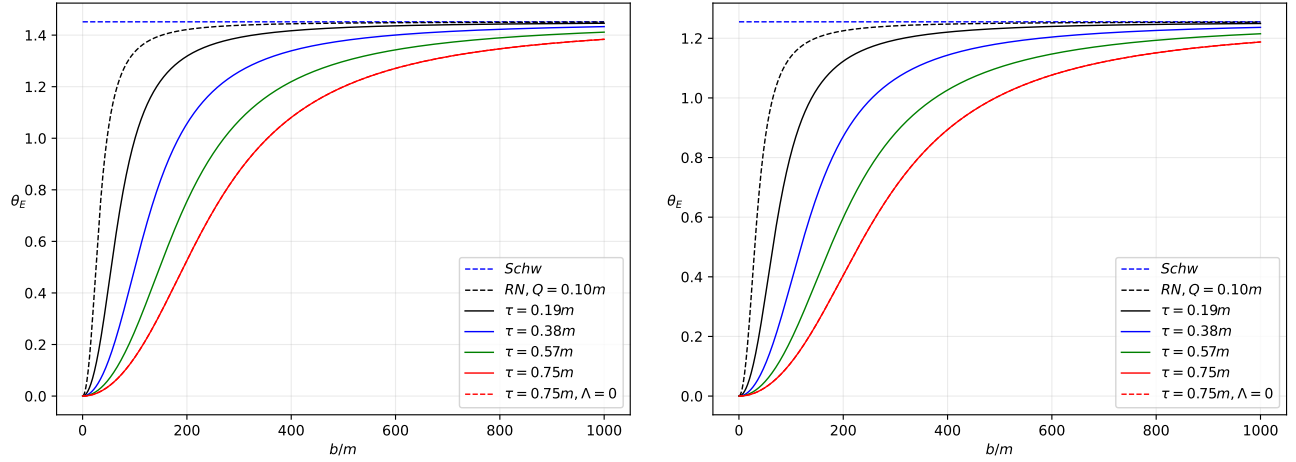


FIG. 5. Plot of the Einstein ring formation for Sgr. A\* (left), and M87\* (right). Here, we assumed that  $Q = 0.10m$ , and  $D_S = D_R$ . The cosmological constant is taken as  $\Lambda \sim 1.1^{-52} \text{ m}^{-2}$

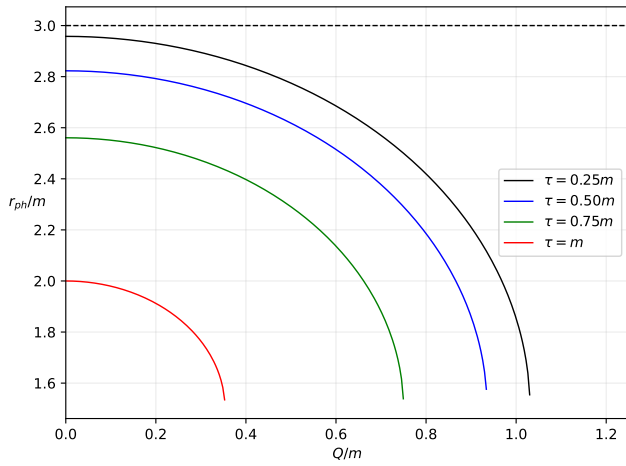


FIG. 6. Location of the photon sphere as  $Q$  varies. These deviations are independent of  $\Lambda$ .

Meanwhile, the theoretical shadow diameter can be obtained via  $d_{\text{sh}}^{\text{theo}} = 2\mathcal{R}_{\text{sh}}$ . Therefore, by using Eq. (53), we get the diameter of the shadow image of M87\* and Sgr. A\* as  $d_{\text{sh}}^{\text{M87*}} = (11 \pm 1.5)m$ , and  $d_{\text{sh}}^{\text{Sgr. A*}} = (9.5 \pm 1.4)m$  respectively. In Fig. 7, we plotted the allowed values of the torsion parameter for a given value of  $Q$  within  $1\sigma$  and  $2\sigma$  from the M87\* and Sgr. A\* data for the shadow diameter. For M87\*, we see that the maximally charge  $Q = m$  is falls below the lower bound of  $2\sigma$ . At  $2\sigma$ , the lower bounds for  $Q = 0.75m, 0.50m, 0.25m$  are  $\tau = 0.66m, 0.87m, 0.97m$  respectively. At  $1\sigma$ , the lower bounds for  $\tau$  only occurs for  $Q = 0.50m, 0.25m$ , which are  $\tau = 0.46m, 0.63m$  respectively. For Sgr. A\*, we see that the case where  $Q = m$  is within the region of  $2\sigma$ . All values of  $Q$  has no lower bound in  $2\sigma$ . In  $1\sigma$ , the lower bounds for  $Q = 0.75m, 0.50m, 0.25m$  are  $\tau = 0.64m, 0.85m, 0.95m$  respectively.

Fig. 8 shows the plot of Eq. (52) for different values of  $\tau$  following the bounds given in Fig. 7. We assumed a value for the black hole charge  $Q = 0.25m$ . Here, the cosmological constant is taken as  $\Lambda \sim \pm 1.1^{-52} \text{ m}^{-2}$  [19]. Overall, we see that the effect of increasing the torsion parameter is to decrease the shadow size relative to the known values in Schwarzschild and RN cases. The vertical dotted line is Earth's location relative to the black holes (M87\* and Sgr. A\*) in units of its mass. The results in the plot suggest such a vast distance is not enough to detect considerably the effects of the cosmological constant to the shadow radius, let alone to consider whether we are in a dS or AdS Universe. However, as can be gleaned, if the location of the observer is near the cosmological horizon, the deviations can be noticeable, especially the difference between the dS and AdS effects.

The plot in Fig. 8 does not reveal the shadow radius behavior when the observer is near the black hole. To reveal this, we scale the cosmological constant to see its overall effect ( $\Lambda = 0.005 \text{ m}^{-2}$ ) and we plot it as shown in Fig. 9. The point  $r_o = 24.5m$  then represents the Hubbles radius. We can see the overall behavior close and cosmologically far from the black hole. In the cosmological distance, the torsion effect in AdS does not seem to vanish and continues to rise relative to the cosmological horizon in the dS case. However, in the dS case, the shadow radius decreases, and the torsion effect is dominated by  $\Lambda$ . In the region close to the black hole, we can see that the torsion effect is little since the effect of the cosmological constant is weak in such regions. The difference between the dS and the Ads case can be so difficult to detect using deviation in the shadow radius at such a location. We can therefore argue that in this scaling, Earth's location is represented somewhere in this region below  $r_o = 3m$ . Finally, we note too that the intersection point in the plot represents the point where  $\alpha_{\text{sh}} = \pi/2$ , where observers can see half of the sky to be dark.

Let us now approximate Eq. (52) due to observers located at the vertical dotted line in Fig. 8. Indeed, at this location

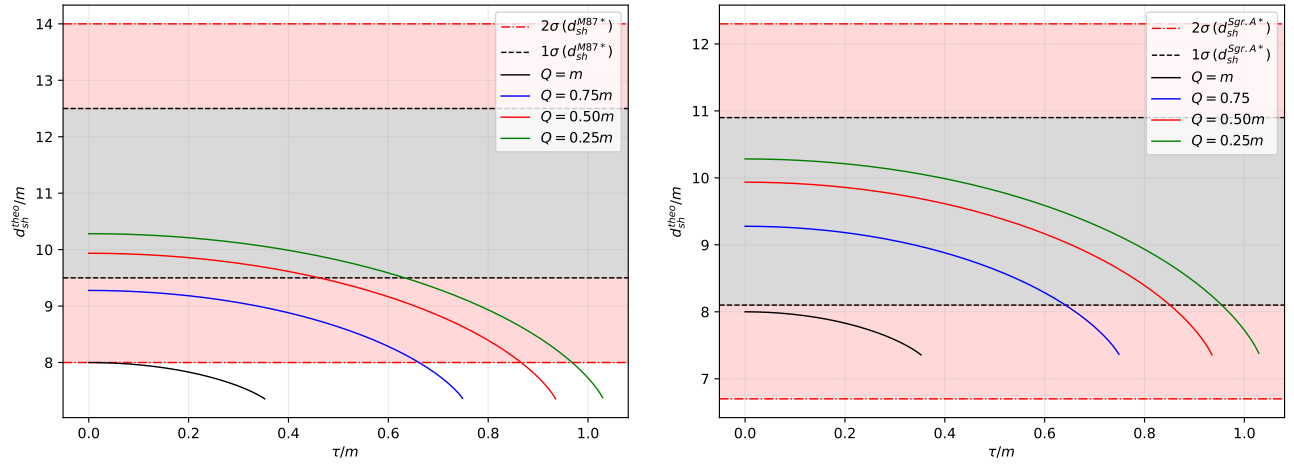


FIG. 7. The variation of the shadow diameter with the torsion parameter  $\tau$  for different values of charge  $Q = m$ (black),  $Q = 0.75m$ (blue),  $Q = 0.50m$ (red) and  $Q = 0.25m$ (green) with  $1\sigma$ (dotted black) and  $2\sigma$ (dot dashed red). Here,  $m$  is the mass of the M87\* or Sgr. A\* black holes. Here, we have used the estimated value of the cosmological constant  $\Lambda \sim -1.1^{-52} \text{ m}^{-2}$ . For instance,  $\Lambda m^2 = 9.217 \times 10^{-27}$  for M87\*, and  $\Lambda m^2 = 4.034 \times 10^{-33}$  for Sgr. A\*.

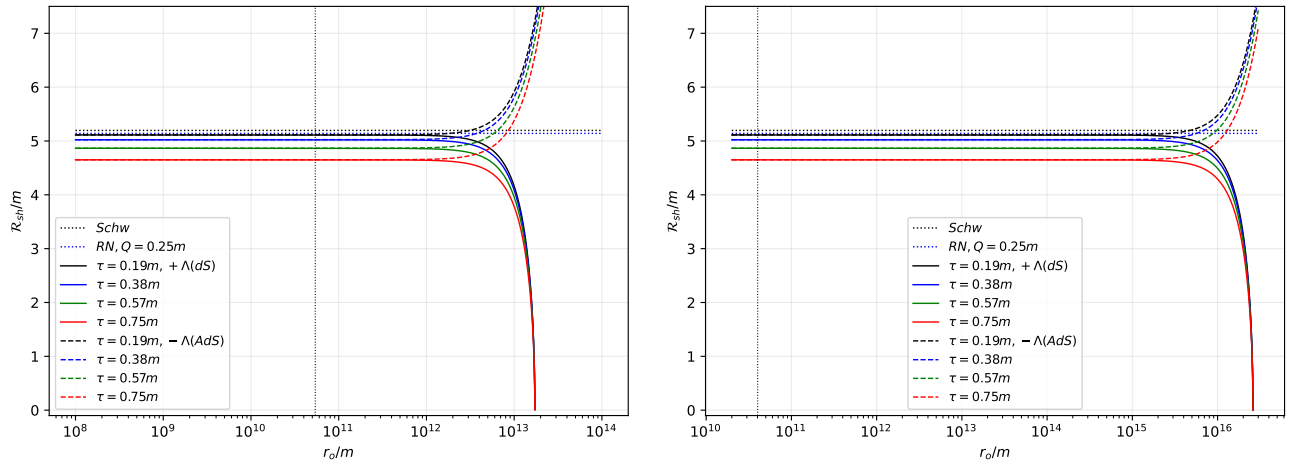


FIG. 8. The behavior of the shadow radius under the effect of the torsion parameter and cosmological constant (M87\* - left, Sgr. A\* - right). The solid line is for the dS case ( $\Lambda > 0$ ), while the dashed line is for the AdS case ( $\Lambda < 0$ ). The dotted vertical line represents our location from the black hole. For M87\* (left),  $r_o = 5.40 \times 10^{10} m$ , while for Sgr. A\* (right)  $r_o = 4.02 \times 10^{10} m$ .

$r_o \gg m$  (same relation to charge and torsion parameters) and following the realistic value of  $\Lambda$  implying  $\Lambda \ll 0$ , the approximation gives

$$\mathcal{R}_{\text{sh}} = 3\sqrt{3}m - \frac{1}{8}\sqrt{3}\Lambda m [4k^2 + 51(\tau^2 + Q^2)], \quad (54)$$

which reduces to the known result in Ref. [19] when  $\tau^2 + Q^2 = 0$ .

The plot in Fig. 8 does not reveal what happens when  $r_o$  is near the black hole. To achieve this, we scale the cosmological constant and set it as  $\Lambda = 0.005 \text{ m}^{-2}$  and plotted as shown in Fig. 9. The point  $r_o \sim 24.5m$  then represents the Hubble's radius. We can then see how the shadow radius behaves near the black hole. The shadow radius decreases as  $r_o/m$  decreases, however, the effect of torsion and cosmological constant in

these regions weakens. At large distances, however, the torsion remains its strong influence in the AdS case, than the dS case.

## V. BEHAVIOR OF THE SHADOW DUE TO A CO-MOVING OBSERVER

In the previous section, it is interesting how the shadow radii behaved due to a static observer at different locations. Here, since we are already incorporating the cosmological constant in this study, let us see how will the shadow radii behave relative to an observer that is co-moving with the cosmic expansion. We will follow the formalism presented in [22]. It all begins with the McVittie metric, and with the inclusion of the

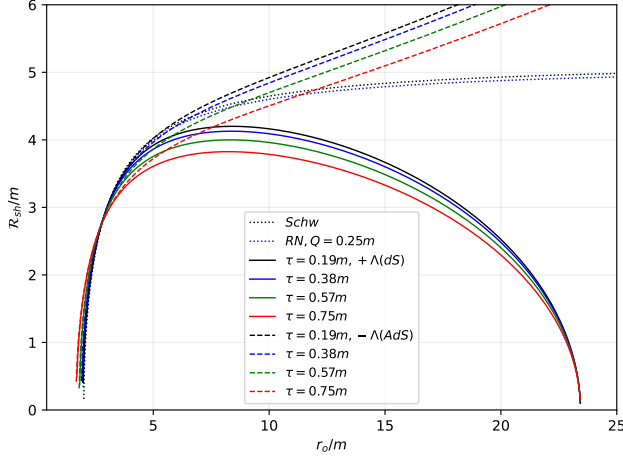


FIG. 9. The behavior of the shadow radius when the cosmological constant is scaled. Here,  $Q = 0.25m$  and  $\Lambda = \pm 0.005 \text{ m}^{-2}$ .

dynamical torsion parameter  $\tau$ , we have [109]:

$$ds^2 = - \left[ \frac{1 - \frac{m^2}{4a(t)^2 r^2} + \frac{\tau^2 + Q^2}{4a(t)^2 r^2}}{\left(1 + \frac{m}{2a(t)r}\right)^2 - \frac{\tau^2 + Q^2}{4a(t)^2 r^2}} \right]^2 dt^2 + a(t)^2 \left[ \left(1 + \frac{m}{2a(t)r}\right)^2 - \frac{\tau^2 + Q^2}{4a(t)^2 r^2} \right]^2 (dr^2 + r^2 d\Omega^2), \quad (55)$$

where  $d\Omega^2 = \sin^2 \vartheta d\varphi^2 + d\vartheta^2$ ,  $a(t) = e^{H_0 t}$  as the scale factor, and  $H_0$  is the present value of the Hubble constant. Note that Eq. (55) is a time-dependent metric. However, if one is close to the black hole, this time dependence vanishes as  $t_0 - t \ll H_0^{-1}$  since the expansion is negligible at such scale [22]. Thus, as  $a(t) \sim a(t_0) = \text{constant}$  and using  $x = a(t_0)r$ , we can write Eq. (55) as

$$ds^2 = - \left[ \frac{1 - \frac{m^2}{4x^2} + \frac{\tau^2 + Q^2}{4x^2}}{\left(1 + \frac{m}{2x}\right)^2 - \frac{\tau^2 + Q^2}{4x^2}} \right]^2 dt^2 + \left[ \left(1 + \frac{m}{2x}\right)^2 - \frac{\tau^2 + Q^2}{4x^2} \right]^2 (dx^2 + x^2 d\Omega^2), \quad (56)$$

which is the RN black hole with torsion in isotropic coordinates. Introducing

$$R = x \left( 1 + \frac{2m}{x} - \frac{\tau^2 + Q^2}{x^2} \right), \quad (57)$$

where in the weak field limit ( $m, \tau, Q \sim 0$ ),  $R \sim x$ , we recover a form similar to the RN metric:

$$ds^2 = - \left( 1 - \frac{2m}{R} + \frac{\tau^2 + Q^2}{R^2} \right) dt^2 + \frac{dR^2}{\left( 1 - \frac{2m}{R} + \frac{\tau^2 + Q^2}{R^2} \right)} + R^2 d\Omega^2. \quad (58)$$

Let the present time be  $t_0$  where the observer is at a radial position  $r_{\text{in}}$ , observing the shadow in strong field limit. The subscript "in" denotes inner region. Then  $x_{\text{in}} = a(t_0)r_{\text{in}}$  and using these variables, we can rewrite Eq. (57) as

$$R_{\text{in}} = x_{\text{in}} \left( 1 + \frac{2m}{x_{\text{in}}} - \frac{\tau^2 + Q^2}{x_{\text{in}}^2} \right). \quad (59)$$

Then using Eq. (58), an observer co-moving with the spacetime in Eq. (56) will then observe the shadow radius  $\mathcal{R}_{\text{in}}$  as

$$\mathcal{R}_{\text{in}} = R_{\text{in}} \sin \alpha_{\text{comov}} = r_{\text{ph}} \left[ \frac{2 \left( 1 - \frac{2m}{R_{\text{in}}} + \frac{\tau^2 + Q^2}{R_{\text{in}}^2} \right)}{1 - \frac{m}{r_{\text{ph}}}} \right]^{1/2}, \quad (60)$$

where  $r_{\text{ph}}$  is still given by Eq. (46). Eq. (60) is the "inner" solution to the shadow radius where the expansion of the Universe is considered to be negligible.

Let us now consider the "outer" region, where the gravitational influence of the black hole is negligible, while the effect of the cosmological expansion is considerable (rapid expansion). In this case, then, the McVittie metric in Eq. (55) will reduce to the FRW metric

$$ds^2 = -dt^2 + a(t)^2 (dr^2 + r^2 d\Omega^2). \quad (61)$$

In this spacetime, effective linear shadow radius  $L_{\text{sh}}$  is given in terms of the angular size of the black hole shadow  $\Psi_{\text{cosmo}}$  as

$$L_{\text{sh}} = \Psi_{\text{cosmo}} D_A(z), \quad (62)$$

where

$$D_A(z) = \frac{1}{1+z} \int_0^z \frac{dk}{H(k)}, \quad (63)$$

and

$$H(k) = H_0 [\Omega_{\text{mat}}(1+k)^3 + \Omega_{\text{rad}}(1+k)^4 + \Omega_{\Lambda}]^{1/2}. \quad (64)$$

Here,  $\Omega_{\text{mat}}, \Omega_{\text{rad}}, \Omega_{\Lambda}$  are present dimensionless density parameters for matter, radiation and dark energy, respectively. Note here that  $\Psi_{\text{cosmo}}$  is so small that the relation  $\sin(\Psi_{\text{cosmo}}) \sim \Psi_{\text{cosmo}}$  applies. Eq. (62) is indeed a function of  $z$  and at such a large distance from the BH,  $x_{\text{out}} \sim R_{\text{out}}$ . Then one can find the connection between  $z$  and  $R_{\text{out}}$  defined by [22]

$$R_{\text{out}} = \int_0^z \frac{dk}{H(k)}. \quad (65)$$

Now, there is a region between the inner and outer regions where the black hole begins to lose influence and at the same point, the cosmological expansion begins to gain influence. Let this "overlapping" region be in  $R_0$  in which, by definition, is still very far from the black hole. If the observer is located at this location at time  $t_0$  where the scale factor is  $a(t_0)$ , then it can be approximated that  $z \ll 1$ . Thus, in this case,  $D_A(z) \sim R_0$  and we then have

$$L_0 = \Psi_0 R_0, \quad (66)$$

which is still equal to the weak field approximation of Eq. (60):

$$\mathcal{R}_o = L_o = 3\sqrt{3}m + \frac{\sqrt{3}(\tau^2 + Q^2)^2}{2} \left[ \frac{1}{m} + \frac{1}{R_o} \right] + \mathcal{O}(R_o^{-2}, R_o^{-3}). \quad (67)$$

$L_o$  is equal to  $L_{sh}$  by matching as pointed out in Ref. [22]. Using  $R_{out}$  instead of  $R_o$ , the effective shadow radius  $\mathcal{R}_{cosmo}$  in the outer region of rapid expansion is then

$$\mathcal{R}_{cosmo} = \Psi_{cosmo} R_{out} = \frac{R_{out}}{D_A(z)} \left[ 3\sqrt{3}m + \frac{\sqrt{3}(\tau^2 + Q^2)^2}{2} \left( \frac{1}{m} + \frac{1}{R_{out}} \right) + \mathcal{O}(R_{out}^{-2}, R_{out}^{-3}) \right]. \quad (68)$$

Finally, the perceived shadow radius  $\mathcal{R}_{approx}$  by an observer co-moving with the cosmic expansion can be approximated through the composite solution [22]:

$$\mathcal{R}_{approx} = \mathcal{R}_{in} + \mathcal{R}_{cosmo} - \mathcal{R}_o. \quad (69)$$

For a Universe dominated by dark energy, we have the following after evaluating Eqs. (63) and (65):

$$D_A(z) = \frac{z}{(1+z)H_0}, \quad R_{out} = \frac{z}{H_0}. \quad (70)$$

Let

$$W = r_{ph} \left[ \frac{2 \left( 1 - \frac{2m}{R_{out}} + \frac{\tau^2 + Q^2}{R_{out}^2} \right)}{1 - \frac{m}{r_{ph}}} \right]^{1/2},$$

$$w = 3\sqrt{3}m + \frac{\sqrt{3}(\tau^2 + Q^2)^2}{2} \left[ \frac{1}{m} + \frac{1}{R_{out}} \right]. \quad (71)$$

Thus, Eq. (69) implies that the approximate shadow radius seen by an observer co-moving with the cosmic expansion is

$$\mathcal{R}_{approx}^\Lambda = W + wH_0R_{out}. \quad (72)$$

In a Universe dominated by matter, we have

$$D_A(z) = \frac{2(\sqrt{z+1}-1)}{H_0(z+1)^{3/2}}, \quad R_{out} = \frac{2(\sqrt{z+1}-1)}{H_0\sqrt{z+1}}, \quad (73)$$

and

$$\mathcal{R}_{approx}^{mat} = W + w \left[ \left( 1 - \frac{H_0 R_{out}}{2} \right)^{-2} - 1 \right]. \quad (74)$$

Finally, radiation dominated Universe gives

$$D_A(z) = \frac{z}{(z+1)^2 H_0}, \quad R_{out} = \frac{z}{(z+1)H_0}, \quad (75)$$

and

$$\mathcal{R}_{approx}^{rad} = W - w \left[ 1 + (R_{out}H_0 - 1)^{-1} \right]. \quad (76)$$

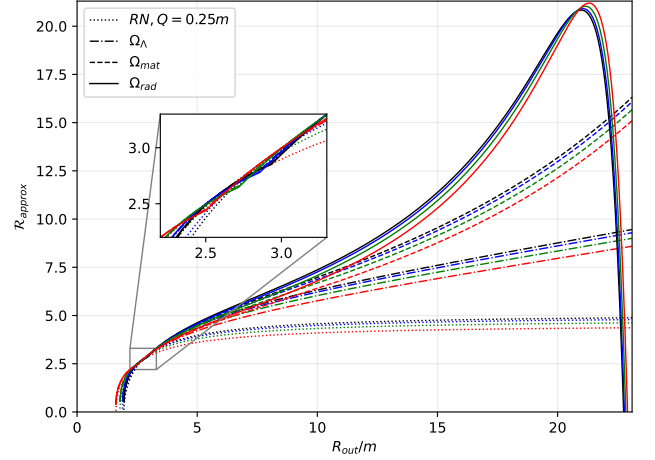


FIG. 10.  $\tau = 0.19$  (black),  $\tau = 0.38$  (blue),  $\tau = 0.57$  (green),  $\tau = 0.75$  (red). Also,  $Q = 0.75M$  and  $H_0 = 0.0408 \text{ m}^{-2}$ .

We plotted Eqs. (72), (74), (76) numerically for an immediate comparison shown in Fig. 10. As can be gleaned from the plot, the overall effect of the torsion parameter even for the co-moving observer is to decrease the shadow radius. Next, the black hole shadow in the radiation-dominated Universe gives the largest deviation, especially near the cosmological horizon. Furthermore, a feature arises due to the existence of the peak value for the shadow radius. The value then drops significantly and intersects with the values for the matter and dark energy-dominated Universes. Thus, observers at this intersection cannot determine using deviations in the shadow radius, whether they are in the radiation-dominated or the matter-dominated (and dark-energy) Universes. Interestingly, for the region between  $2.5m < R_{out} < 3.0m$  (see inset plot), the deviation caused by these types of Universes for the co-moving observer's perception of the shadow is nearly negligible since we can still see some tiny deviation to the pure RN type case. Thus, relating Fig. 10 to Figs. 8 and 9, Earth's co-moving location is in the region where the effect of the cosmological constant is again small. Based on the inset plot, however, the tiny deviation caused by the effect of co-moving motion can still be possibly detected, and as to which type of Universe we are in is very hard to tell in the context of observing the black hole shadow.

## VI. SPHERICALLY INFALLING ACCRETION

The actual image of the black hole is not observed as the visible boundary within the static accretion disk model. However, in the more realistic scenario, the accretion disk also moves around the black hole and provides a synchrotron emission from accumulation. In this section, we study spherically free-falling accretion onto a black hole from infinity by applying a realistic model to visualize the shadow using the method defined in [110, 111].

First, we study the specific intensity observed at the observed

photon frequency  $\nu_{\text{obs}}$  by solving this integral along the light ray:

$$I(\nu_{\text{obs}}, b_\gamma) = \int_\gamma g^3 j(\nu_e) dl_{\text{prop}}, \quad (77)$$

where  $j(\nu_e)$  is the emissivity per unit volume,  $b_\gamma$  is the impact parameter,  $\nu_e$  is the photon frequency of the emitter, and  $dl_{\text{prop}}$  is the infinitesimal proper length. Here we define the redshift factor for the infalling accretion as follows:

$$g = \frac{k_\mu u_o^\mu}{k_\mu u_e^\mu}, \quad (78)$$

where the 4-velocity of the photon is  $k^\mu = \dot{x}^\mu$  and 4-velocity of the distant observer is  $u_o^\mu = (1, 0, 0, 0)$ . Moreover, the  $u_e^\mu$  stands for the 4-velocity of the infalling accretion

$$u_e^t = \frac{1}{A(r)}, \quad u_e^r = -\sqrt{\frac{1-A(r)}{A(r)B(r)}}, \quad u_e^\theta = u_e^\phi = 0. \quad (79)$$

Using the relation of  $k_\alpha k^\alpha = 0$ , one can derive  $k_r$  and  $k_t$  which is a constant of motion for the photons:

$$k_r = \pm k_t \sqrt{B(r) \left( \frac{1}{A(r)} - \frac{b^2}{r^2} \right)}. \quad (80)$$

Note that sign of  $\pm$  shows that the photon gets close to (away from) the black hole. Then the redshift factor  $g$  and proper distance  $dl_\gamma$  can be written as follows

$$g = \left( u_e^t + \frac{k_r}{k_t} u_e^r \right)^{-1}, \quad (81)$$

and

$$dl_\gamma = k_\mu u_e^\mu d\lambda = \frac{k^t}{g|k_r|} dr. \quad (82)$$

We then consider only the monochromatic emission for the specific emissivity with rest-frame frequency  $\nu_*$  as follows:

$$j(\nu_e) \propto \frac{\delta(\nu_e - \nu_*)}{r^2}. \quad (83)$$

Afterwards, the intensity equation given in (77) become

$$F(b_\gamma) \propto \int_\gamma \frac{g^3}{r^2} \frac{k_e^t}{k_e^r} dr. \quad (84)$$

We investigate the shadow cast with the thin-accretion disk of the black hole in quadratic Poincare gauge gravity with massive torsion. First of all, the above integral is solved numerically by using the Okyay-Övgün *Mathematica* notebook package [75], (used in [68, 78, 79]). We integrate the flux to see the effects of the parameters of the dynamical torsion  $\tau$ . Then we plot the intensity for various values of the dynamical torsion parameter  $\tau$  versus  $b$  observed by the distant observer in Figs. (11, 12 and 13).

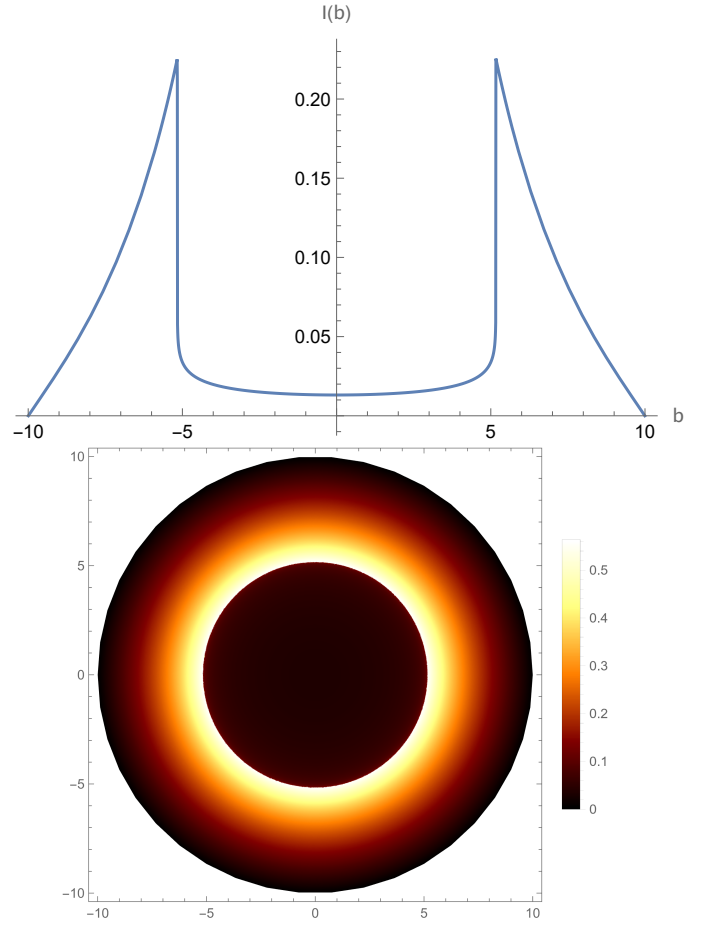


FIG. 11. The specific intensity  $I_{\text{obs}}$  seen by a distant observer for an infalling accretion at fixed  $\Lambda = 0$ , and  $\tau = 0.19m$ .

It is seen in figures that when  $b$  increases, intensity becomes larger first, then hit the peak value sharply at the photon sphere where the photons are captured by a black hole quickly, and then smoothly decrease. Below the intensity figures, the shadow cast of the black hole is shown as the two-dimensional image with a photon sphere by a distant observer in  $(X, Y)$  plane. Note that at the center of the black hole there is a black region (known as the event horizon) which is bounded by a bright ring (known as a photon sphere with the strongest luminosity). There is also a maximum luminosity region after that brightness lowers gradually. Here we observe that the luminosity of the shadow cast increases with increasing the value of the dynamical torsion parameter  $\tau$  as seen in Fig. 13.

## VII. QUASINORMAL MODES IN EIKONOL LIMIT

Since the first detection of gravitational waves (GWs) from the coalescence of two stellar-mass black holes in 2015 by the LIGO/VIRGO collaborations [3], gravitational wave physics has begun. Then wealth of data from gravitational waves are analyzed to test alternative theories of gravity and different

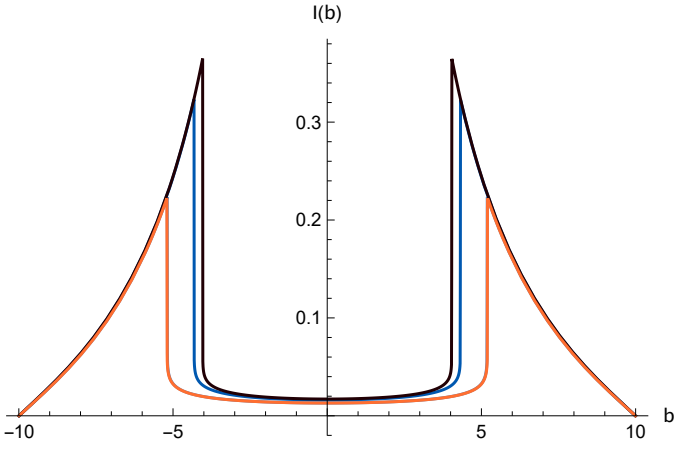


FIG. 12. The specific intensity  $I_{\text{obs}}$  seen by a distant observer for an infalling accretion at fixed  $\Lambda = 0$ ,  $\tau = 0.99m$  (black),  $\tau = 0.38m$  (blue), and  $\tau = 0.10m$  (orange).

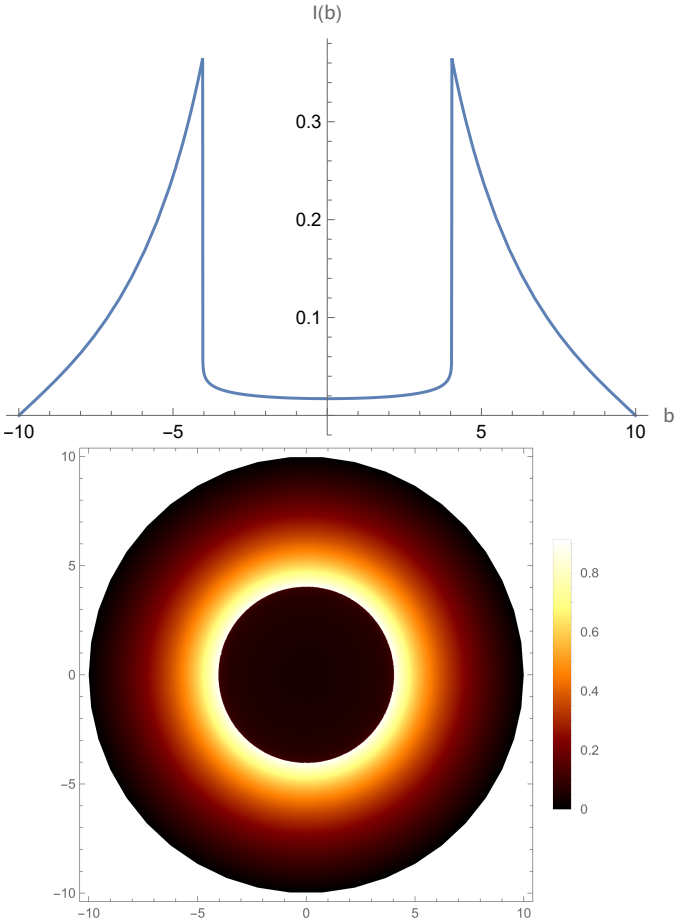


FIG. 13. The specific intensity  $I_{\text{obs}}$  seen by a distant observer for an infalling accretion at fixed  $\Lambda = 0$ , and  $\tau = 0.99m$ .

models of compact objects. Perturbative analysis of black hole spacetimes dominated by ‘quasinormal ringing’ is used to do this. Quasi-normal modes (QNMs) are oscillations with complex frequencies with energy dissipation. The complex frequencies of QNMs have the characteristic properties of the BHs such as mass, charge, and angular momentum, independent of the initial perturbations. To do so, first, we use the following spherical symmetric spacetime:

$$ds^2 = -f(r)dt^2 + \frac{dr^2}{f(r)} + h^2(r)(d\theta^2 + \sin^2\theta d\varphi^2), \quad (85)$$

where  $f(r)$  and  $h^2(r)$ . The general covariant equations for the scalar  $\Phi$  and electromagnetic  $A_\mu$  fields are written as follows:

$$\begin{aligned} \frac{1}{\sqrt{-g}}\partial_\mu(\sqrt{-g}g^{\mu\nu}\partial_\nu\Phi) &= 0 \\ \frac{1}{\sqrt{-g}}\partial_\mu(F_{\rho\sigma}g^{\rho\nu}g^{\sigma\mu}\sqrt{-g}) &= 0, \end{aligned} \quad (86)$$

where  $F_{\mu\nu} = \partial_\mu A_\nu - \partial_\nu A_\mu$ .

After solving the above equations on the background of black hole spacetime Eq. (85), and separate the variables, Eq. (86) reduce to the Schrodinger-like form with the tortoise coordinate  $r_*$  defined by  $dr_*/dr = 1/f(r)$ . Note that  $\Psi_s$  stands for the scalar or vector field oscillating and decaying at a complex frequency  $\omega$ , and  $V_s$  is the spin-dependent Regge-Wheeler (RW) potential. First, let us consider a massless scalar ( $s = 0$ ) perturbation field with its wave equation:

$$\frac{1}{\sqrt{-g}}\partial_\mu(\sqrt{-g}g^{\mu\nu}\partial_\nu\phi) = 0, \quad (87)$$

in which  $g$  is the determinant. After we decompose  $\phi(t, r, \theta, \varphi)$  into Fourier modes,

$$\phi(t, r, \theta, \varphi) = \sum_{\ell, m} e^{-i\omega t} \frac{\Psi_{s=0}(r)}{h(r)} Y_{\ell m}(\theta, \varphi), \quad (88)$$

and redefine  $\Psi_{s=0}(r)$  as the perturbation field, where  $Y_{\ell m}(\theta, \varphi)$  (for the spherical harmonics). Note that near the event horizon, solutions must be purely ingoing, and at spatial infinity, solutions must be purely outgoing for asymptotically flat or de Sitter solutions, but different in AdS because AdS has a timelike boundary). Then we substitute the decomposition Eq. (88) into Eq. (87), and find master equation for  $\Psi_{s=0}(r)$  with the RW potential,

$$V_{s=0} = f(r) \left\{ \frac{\ell(\ell+1)}{h^2(r)} + \frac{1}{h(r)} \frac{d}{dr} \left[ f(r) \frac{dh(r)}{dr} \right] \right\}. \quad (89)$$

For a linearized Maxwell ( $s = 1$ ) field perturbation, we can obtain the RW potential in a similar way to the scalar field, or one can derive the RW potential of the spin-1 field using the formalism developed in Ref. [112]:

$$V_{s=1} = f(r) \left[ \frac{\ell(\ell+1)}{h^2(r)} \right]. \quad (90)$$

Hence, for the spacetime defined in (85), the master equation with the spin-dependent RW potential for the massless scalar

( $s = 0$ ) and for the electromagnetic ( $s = 1$ ) field perturbations can be written in compact form as follows ( $l = 1, 2, 3$  is multipole number, and  $\omega = \omega_R - i\omega_I$  is a complex quasinormal mode frequency) [113–115]:

$$V_s = f(r) \left\{ \frac{\ell(\ell+1)}{h^2(r)} + \frac{(1-s)}{h(r)} \frac{d}{dr} \left[ f(r) \frac{dh(r)}{dr} \right] \right\}. \quad (91)$$

Further in this section, we use the method of eikonal (geometric optics) limit (unstable circular null geodesic method) to derive the QNMs [116, 117]. The imaginary part of the quasinormal mode frequency ( $\text{Im } \omega = -\omega_I$ ) which is responsible for the temporal, exponential decay can be calculated, in the large- $l$  limit ( $l \rightarrow \infty$ ) (only the  $g_{tt}$  component is relevant) [118, 119] i.e. as the angular momentum number describing our mode solution becomes very large, as follows:

$$\omega_{l \gg 1} = l\Omega_{\text{ph}} - i \left( n + \frac{1}{2} \right) |\lambda_L|, \quad (92)$$

with the angular velocity  $\Omega_{\text{ph}}$ :

$$\Omega_{\text{ph}} = \frac{\sqrt{-g_{tt}(r_{\text{ph}})}}{r_{\text{ph}}} = \frac{\sqrt{f(r_{\text{ph}})}}{r_{\text{ph}}}, \quad (93)$$

and Lyapunov exponent  $\lambda_L$ :

$$\lambda_L = \sqrt{\frac{f(r_{\text{ph}}) \left[ 2f(r_{\text{ph}}) - r_{\text{ph}}^2 f''(r_{\text{ph}}) \right]}{2r_{\text{ph}}^2}}, \quad (94)$$

where  $n$  is the overtone number and take values  $n = 0, 1, 2, \dots$ . Note that the eikonal limit is independent of the spin of the perturbation, so that scalar, electromagnetic, and gravitational perturbations of black holes give the same behavior in the eikonal limit [120]. We show our results in Table I that the real parts increase, but the imaginary part of the QNMs decrease with the increasing dynamical torsion parameter  $\tau$ . We can conclude that these modes are stable cause the imaginary parts of the QNMs frequencies ( $\text{Im } \omega = -\omega_I$ ) are negative. We can say that when the dynamical torsion parameter  $\tau$  increases, the scalar perturbations oscillate with lower frequency  $\omega$  which means that oscillates decay slowly.

$\tau/m$	$\omega_R$	$\omega_I$
0.06	0.192572	0.865842
0.12	0.192922	0.865315
0.18	0.193511	0.864422
0.24	0.194299	0.863216

TABLE I. Effects of the torsion parameter  $\tau$  on the quasinormal modes frequencies in eikonal limits for fixed  $\Lambda = 0$ ,  $Q = 0.02m$ ,  $s = 1$ ,  $n = 0$ , and  $l = 1$ .

### VIII. BOUNDS OF GREYBODY FACTORS AND HIGH-ENERGY ABSORPTION CROSS-SECTION VIA SINC APPROXIMATION

In this section, we calculate the bound for the greybody factor of the black hole with dynamical torsion by using the

rigorous lower bound to probe the effect of  $\tau$  on the bound. Authors in [121, 122] give the rigorous bound of greybody factor as follows [121, 122]:

$$T_b \geq \text{sech}^2 \left( \frac{1}{2\omega} \int_{-\infty}^{\infty} |V| \frac{dr}{f(r)} \right). \quad (95)$$

In the previous section, we give the RW potential for the massless scalar field, and using it we can calculate the bound as follows:

$$T \geq T_b = \text{sech}^2 \left[ \frac{-\frac{2(\tau^2+Q^2)}{3r_{\text{outer}}^3} + \frac{l(l+1)}{r_{\text{outer}}} + \frac{m}{r_{\text{outer}}^2}}{2\omega} \right]. \quad (96)$$

Note that this bound reduces to the Schwarzschild case at  $(\tau, Q) \rightarrow 0$  correctly, as  $T_{\text{Sch}} \geq \text{sech}^2 \left( \frac{2l(l+1)+1}{8m\omega} \right)$ . To show the effect of dynamical torsion on the greybody bound of the black hole, we plot it in Fig. 14 (Scalar Field). Similarly, using the RW potential for the em field from last section, we calculate the bound as follows:

$$T \geq T_b = \text{sech}^2 \left[ \frac{l(l+1)}{2\omega \left( \sqrt{-\tau^2 - Q^2} + m^2 + m \right)} \right], \quad (97)$$

then we plot it to show the effect of the dynamical torsion parameter on the greybody factor in Fig. 14 (EM field). Then we plot the greybody bound versus the  $\omega$  for different values of  $s$  to show the effect of the spin where increase the bound when spin number increases from zero to two in Fig. 15.

Lastly, we calculate the high-energy absorption cross-section via Sinc approximation. First, Sanchez studied the absorption cross-section for the Schwarzschild black hole in the high-frequency regime and it was shown that increasing the frequency for the ordinary material sphere, monotonically increase the absorption cross-section oscillated around the constant geometric-optics value for the black hole (related to the photon sphere) [123]. Then the relation between the impact parameter and cross-section of the photon sphere is given at critical values and limiting the value of the absorption cross-section. One can conclude at low energy scales, it is the characteristic properties of BH and the cross-section equals to BH area [124]. On the other hand, at high energies using the geometrical cross-section of the photon sphere can be studied using the complex angular momentum technique [125]. Decanini et al. use the Regge pole techniques to prove the oscillatory pattern of the high-energy absorption cross-section related to a Sinc(x) function including the photon sphere.

At high frequency, the absorption cross section is approximately equal to classical capture cross section of null geodesics:  $\sigma_{\text{geo}} = \pi b_{\text{crit}}^2$  with the critical impact parameter  $b_{\text{crit}}$ . Then one can calculate the oscillatory part of the absorption cross section in the eikonal limit as follows [125]:

$$\sigma_{\text{osc}} = -4\pi \frac{\lambda b_{\text{crit}}^2}{\omega} e^{-\pi \lambda_L b_{\text{crit}}} \sin \frac{2\pi w}{\Omega_{\text{ph}}}, \quad (98)$$

where  $\lambda_L$  is known as the Lyapunov exponent given in Eq. (94) and angular velocity is  $\Omega_{\text{ph}}$  with the radius of the photon

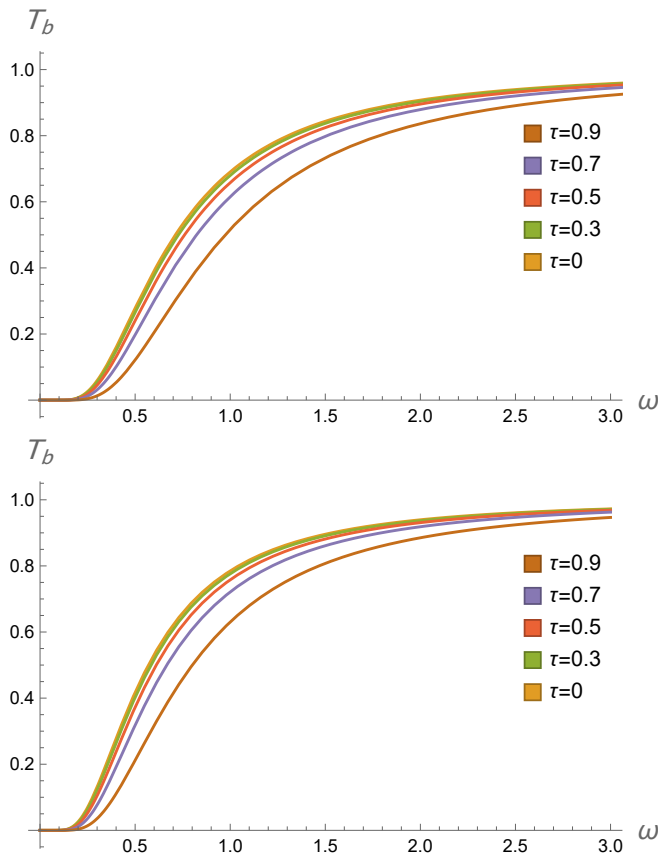


FIG. 14. (Scalar Field) The Greybody Bound  $T_b$  versus the  $\omega$  for different values of torsion charge, with  $m = 2$ ,  $l = 1$ ,  $s = 0$ , and  $Q = 0.18m$ . (EM Field) The Greybody Bound  $T_b$  versus the  $\omega$  for different values of torsion charge  $\tau$ , with  $m = 2$ ,  $l = 1$ ,  $s = 1$ , and  $Q = 0.18m$ .

sphere  $r_{\text{ph}}$ . Hence, the Sinc approximation said that the total absorption cross section at the eikonal limit is  $\sigma_{\text{abs}} \approx \sigma_{\text{osc}} + \sigma_{\text{geo}}$  [123, 125–130]. In the Fig. 16 we plot the total absorption cross section for various values of  $\tau$ . It can be seen that as the values of dynamical torsion parameter increase, the total absorption cross section decreases. Moreover, there is a regular oscillatory behavior around the high-frequency limit.

## IX. CONCLUSION

In the present work, we have analyzed the effect of the torsion effect in correspondence with the RN geometries with cosmological constant within the framework of PG theory with massive torsion, first, to the weak deflection angle of massive and null particles. Our findings indicate that, in general, increasing the value of the torsion parameter decreases the value of the weak deflection angle, and its effect diminishes at distances comparable to the cosmological horizon. In addition, both the dS and AdS cases gave interesting and unique differences in the behavior of the weak deflection angle. First, the deflection angle of massive particles can give more detectabil-

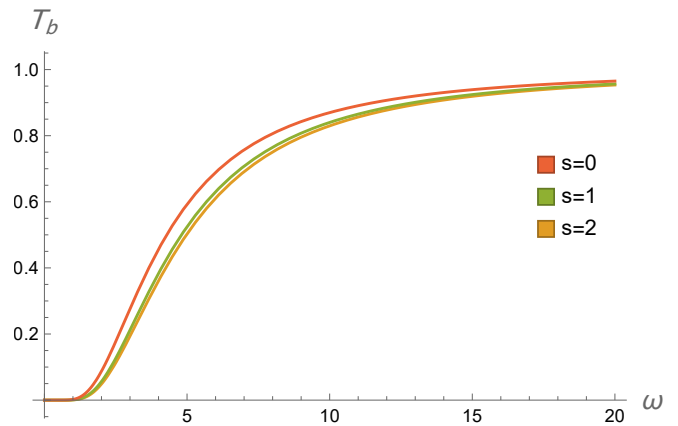


FIG. 15. The Greybody Bound  $T_b$  versus the  $\omega$  for different values of the  $s$ , with  $\tau = 0.9m$ ,  $m = 2$ ,  $l = 1$ ,  $s = 1$ , and  $Q = 0.18m$ .

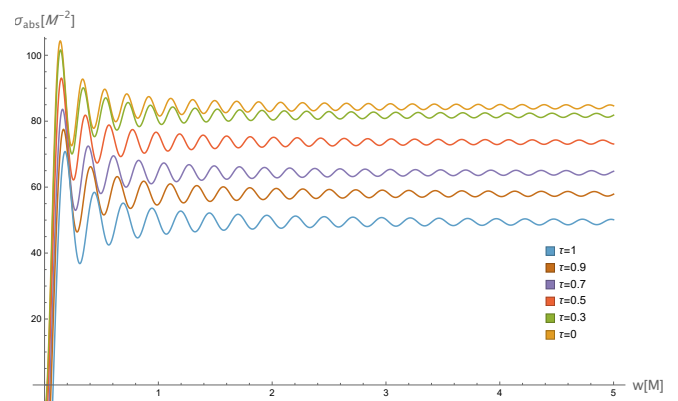


FIG. 16. The total absorption cross section for various values of the torsion charge  $\tau$ , with  $m = 2$ , and  $Q = 0.18m$ .

ity due to a higher value of  $\alpha$  as compared to the null particles, especially in the AdS case. For a receiver near the black hole (Fig. 2),  $\alpha$  is lesser compared to the receiver far from the black hole (Fig. 3). Such a higher value of  $\alpha$  is compensated by the ability to detect positive deflection angles at larger distances. Intuitively, we should expect that the effect of the cosmological constant will manifest greatly at distances comparable to the cosmological horizon. However, in the case of the weak deflection angle, its effect already manifests greatly for receivers with considerable distance from the BH.

Meanwhile, the behavior of the shadow radius was also examined. The main result of the study, for the torsion effect, is similar to the  $\alpha$ . More interestingly, considering the Earth's location from the known BHs in our galaxy and M87, we find that the black hole shadow does not react strongly to the cosmological background, unlike in  $\hat{\alpha}$ . Nonetheless, the effect is magnified near the cosmological horizon. We also see differing behavior when compared to the AdS case. We also considered the co-moving case, for dark energy, matter, and radiation-dominated Universes. We get similar observations at cosmological distances. Comparable to Earth's location, however, we can potentially detect a deviation in the shadow,

but it will be difficult to differentiate between which type of Universe we live in.

To broaden the scope of the study, we have also analyzed the effects of the torsion parameter on the shadow with infalling spherical accretion. We have shown that the dynamical torsion parameter  $\tau$  has some positive impact on the luminosity of the photon sphere for the infalling spherical accretion model. The luminosity of the photon sphere around the black hole horizon increases gradually with increased dynamical torsion parameter  $\tau$  shown in Figs. (11, 12 and 13). Moreover, we have calculated the quasinormal modes in the eikonal limit and showed our results in Table I that the real parts increase, but the

imaginary part of the QNMs decrease with the increasing dynamical torsion parameter  $\tau$ . Last, we have obtained greybody bounds and the high-energy absorption cross-section via Sinc approximation in the high-frequency regime and have shown how the dynamical torsion parameter  $\tau$  affects them in Figs. 14, 15, 16. The difference in dynamical torsion parameter  $\tau$  is indeed visible.

Future prospects include extending the study to obtain the rotating solution of the metric in Eq. (2). It would also be interesting to find the exact form of the shadow radius expression for an observer that is co-moving with the cosmological expansion.

- 
- [1] A. Einstein, *Annalen Phys.* **49**, 769 (1916).
- [2] F. W. Dyson, A. S. Eddington, and C. Davidson, *Phil. Trans. Roy. Soc. Lond. A* **220**, 291 (1920).
- [3] B. P. Abbott *et al.* (LIGO Scientific, Virgo), *Phys. Rev. Lett.* **116**, 061102 (2016), arXiv:1602.03837 [gr-qc].
- [4] K. Akiyama *et al.* (Event Horizon Telescope), *Astrophys. J. Lett.* **875**, L1 (2019), arXiv:1906.11238 [astro-ph.GA].
- [5] K. Akiyama *et al.* (Event Horizon Telescope), *Astrophys. J. Lett.* **930**, L12 (2022).
- [6] H. Weyl, *Zeitschrift fur Physik* **56**, 330 (1929).
- [7] E. Cartan, A. Magnon, A. Ashtekar, and A. Trautman, *On Manifolds with an Affine Connection and the Theory of General Relativity*, Lecture notes (Bibliopolis, 1986).
- [8] V. Fock, *Zeitschrift fur Physik* **57**, 261 (1929).
- [9] R. Utiyama, *Phys. Rev.* **101**, 1597 (1956).
- [10] D. W. Sciama, in *Recent Developments in General Relativity* (1962) p. 415.
- [11] T. W. B. Kibble, *J. Math. Phys.* **2**, 212 (1961).
- [12] M. Blagojevic and F. W. Hehl, (2012), arXiv:1210.3775 [gr-qc].
- [13] F. W. Hehl, P. Von Der Heyde, G. D. Kerlick, and J. M. Nester, *Rev. Mod. Phys.* **48**, 393 (1976).
- [14] J. A. R. Cembranos and J. Gigante Valcarcel, *Phys. Lett. B* **779**, 143 (2018), arXiv:1708.00374 [gr-qc].
- [15] K.-J. He, S.-C. Tan, and G.-P. Li, *Eur. Phys. J. C* **82**, 81 (2022).
- [16] I. Gkigkitzis, I. Haranas, and E. Cavan, *Ukr. J. Phys.* **64**, 683 (2019).
- [17] V. Nikiforova, *Phys. Rev. D* **102**, 124007 (2020), arXiv:2010.05910 [gr-qc].
- [18] F. Kottler, *Annalen der Physik* **361**, 401 (1918).
- [19] V. Perlick, O. Y. Tsupko, and G. S. Bisnovaty-Kogan, *Phys. Rev. D* **97**, 104062 (2018).
- [20] G. S. Bisnovaty-Kogan and O. Y. Tsupko, *Phys. Rev. D* **98**, 084020 (2018), arXiv:1805.03311 [gr-qc].
- [21] J. T. Firouzjaee and A. Allahyari, *Eur. Phys. J. C* **79**, 930 (2019), arXiv:1905.07378 [astro-ph.CO].
- [22] O. Y. Tsupko and G. S. Bisnovaty-Kogan, *International Journal of Modern Physics D* **29**, 2050062 (2020).
- [23] R. V. Maluf and J. C. S. Neves, *Phys. Rev. D* **103**, 044002 (2021), arXiv:2011.12841 [gr-qc].
- [24] J. L. Synge, *Mon. Not. R. Astron. Soc.* **131**, 463 (1966).
- [25] J. P. Luminet, *Astron. Astrophys.* **75**, 228 (1979).
- [26] C. A. R. Herdeiro, A. M. Pombo, E. Radu, P. V. P. Cunha, and N. Sanchis-Gual, *JCAP* **04**, 051 (2021), arXiv:2102.01703 [gr-qc].
- [27] P. V. P. Cunha, N. A. Eiró, C. A. R. Herdeiro, and J. P. S. Lemos, *JCAP* **03**, 035 (2020), arXiv:1912.08833 [gr-qc].
- [28] P. V. P. Cunha, C. A. R. Herdeiro, and E. Radu, *Universe* **5**, 220 (2019), arXiv:1909.08039 [gr-qc].
- [29] P. V. P. Cunha and C. A. R. Herdeiro, *Gen. Rel. Grav.* **50**, 42 (2018), arXiv:1801.00860 [gr-qc].
- [30] P. V. P. Cunha, C. A. R. Herdeiro, B. Kleihaus, J. Kunz, and E. Radu, *Phys. Lett. B* **768**, 373 (2017), arXiv:1701.00079 [gr-qc].
- [31] F. H. Vincent, E. Gourgoulhon, C. Herdeiro, and E. Radu, *Phys. Rev. D* **94**, 084045 (2016), arXiv:1606.04246 [gr-qc].
- [32] M. Afrin, R. Kumar, and S. G. Ghosh, *Mon. Not. Roy. Astron. Soc.* **504**, 5927 (2021), arXiv:2103.11417 [gr-qc].
- [33] S. K. Jha and A. Rahaman, (2021), arXiv:2111.02817 [gr-qc].
- [34] M. Khodadi, G. Lambiase, and D. F. Mota, *JCAP* **09**, 028 (2021), arXiv:2107.00834 [gr-qc].
- [35] M. Khodadi, A. Allahyari, S. Vagnozzi, and D. F. Mota, *JCAP* **09**, 026 (2020), arXiv:2005.05992 [gr-qc].
- [36] R. Kumar and S. G. Ghosh, *Astrophys. J.* **892**, 78 (2020), arXiv:1811.01260 [gr-qc].
- [37] R. Kumar and S. G. Ghosh, *JCAP* **07**, 053 (2020), arXiv:2003.08927 [gr-qc].
- [38] X.-X. Zeng, H.-Q. Zhang, and H. Zhang, *Eur. Phys. J. C* **80**, 872 (2020), arXiv:2004.12074 [gr-qc].
- [39] K.-J. He, S.-C. Tan, and G.-P. Li, *Eur. Phys. J. C* **82**, 81 (2022).
- [40] V. I. Dokuchaev and N. O. Nazarova, *Universe* **6**, 154 (2020), arXiv:2007.14121 [astro-ph.HE].
- [41] S. Vagnozzi, R. Roy, Y.-D. Tsai, and L. Visinelli, (2022), arXiv:2205.07787 [gr-qc].
- [42] R. Roy, S. Vagnozzi, and L. Visinelli, *Phys. Rev. D* **105**, 083002 (2022), arXiv:2112.06932 [astro-ph.HE].
- [43] S. Vagnozzi and L. Visinelli, *Phys. Rev. D* **100**, 024020 (2019), arXiv:1905.12421 [gr-qc].
- [44] A. Allahyari, M. Khodadi, S. Vagnozzi, and D. F. Mota, *JCAP* **02**, 003 (2020), arXiv:1912.08231 [gr-qc].
- [45] C. Bambi, K. Freese, S. Vagnozzi, and L. Visinelli, *Phys. Rev. D* **100**, 044057 (2019), arXiv:1904.12983 [gr-qc].
- [46] Y. Meng, X.-M. Kuang, and Z.-Y. Tang, (2022), arXiv:2204.00897 [gr-qc].
- [47] C.-Y. Chen, (2022), arXiv:2205.06962 [gr-qc].
- [48] Y. Chen, R. Roy, S. Vagnozzi, and L. Visinelli, (2022), arXiv:2205.06238 [astro-ph.HE].
- [49] M. Wang, S. Chen, and J. Jing, (2022), arXiv:2205.05855 [gr-qc].
- [50] T. Bronzwaer and H. Falcke, *Astrophys. J.* **920**, 155 (2021), arXiv:2108.03966 [astro-ph.HE].
- [51] H. Falcke, F. Melia, and E. Agol, *Astrophys. J. Lett.* **528**, L13

- (2000), [arXiv:astro-ph/9912263](#).
- [52] F. Atamurotov, A. Abdujabbarov, and B. Ahmedov, *Phys. Rev. D* **88**, 064004 (2013).
- [53] A. A. Abdujabbarov, L. Rezzolla, and B. J. Ahmedov, *Mon. Not. Roy. Astron. Soc.* **454**, 2423 (2015), [arXiv:1503.09054 \[gr-qc\]](#).
- [54] S.-W. Wei, Y.-C. Zou, Y.-X. Liu, and R. B. Mann, *JCAP* **08**, 030 (2019), [arXiv:1904.07710 \[gr-qc\]](#).
- [55] S.-W. Wei, Y.-X. Liu, and R. B. Mann, *Phys. Rev. D* **99**, 041303 (2019), [arXiv:1811.00047 \[gr-qc\]](#).
- [56] S. Abdolrahimi, R. B. Mann, and C. Tzounis, *Phys. Rev. D* **91**, 084052 (2015), [arXiv:1502.00073 \[gr-qc\]](#).
- [57] C. Adair, P. Bueno, P. A. Cano, R. A. Hennigar, and R. B. Mann, *Phys. Rev. D* **102**, 084001 (2020), [arXiv:2004.09598 \[gr-qc\]](#).
- [58] S. Abdolrahimi, R. B. Mann, and C. Tzounis, *Phys. Rev. D* **92**, 124011 (2015), [arXiv:1510.03530 \[gr-qc\]](#).
- [59] R. A. Konoplya and A. F. Zinhailo, *Eur. Phys. J. C* **80**, 1049 (2020), [arXiv:2003.01188 \[gr-qc\]](#).
- [60] R. A. Konoplya, *Phys. Lett. B* **795**, 1 (2019), [arXiv:1905.00064 \[gr-qc\]](#).
- [61] R. A. Konoplya, *Phys. Lett. B* **804**, 135363 (2020), [arXiv:1912.10582 \[gr-qc\]](#).
- [62] R. Shaikh, P. Kocherlakota, R. Narayan, and P. S. Joshi, *Mon. Not. Roy. Astron. Soc.* **482**, 52 (2019), [arXiv:1802.08060 \[astro-ph.HE\]](#).
- [63] R. Shaikh, *Phys. Rev. D* **100**, 024028 (2019), [arXiv:1904.08322 \[gr-qc\]](#).
- [64] F. Rahaman, K. N. Singh, R. Shaikh, T. Manna, and S. Aktar, *Class. Quant. Grav.* **38**, 215007 (2021), [arXiv:2108.09930 \[gr-qc\]](#).
- [65] A. Belhaj, M. Benali, A. El Balali, H. El Moumni, and S. E. Ennadifi, *Class. Quant. Grav.* **37**, 215004 (2020), [arXiv:2006.01078 \[gr-qc\]](#).
- [66] A. Belhaj, H. Belmahi, M. Benali, W. El Hadri, H. El Moumni, and E. Torrente-Lujan, *Phys. Lett. B* **812**, 136025 (2021), [arXiv:2008.13478 \[hep-th\]](#).
- [67] A. Belhaj, H. Belmahi, and M. Benali, *Phys. Lett. B* **821**, 136619 (2021), [arXiv:2110.06771 \[hep-th\]](#).
- [68] L. Chakhchi, H. El Moumni, and K. Masmar, *Phys. Rev. D* **105**, 064031 (2022).
- [69] V. Perlick, O. Y. Tsupko, and G. S. Bisnovaty-Kogan, *Phys. Rev. D* **97**, 104062 (2018), [arXiv:1804.04898 \[gr-qc\]](#).
- [70] V. Perlick and O. Y. Tsupko, *Phys. Rept.* **947**, 1 (2022), [arXiv:2105.07101 \[gr-qc\]](#).
- [71] R. C. Pantig and E. T. Rodulfo, *Chinese J. Phys.* **68**, 236 (2020).
- [72] R. E. T. Pantig Reggie C., Yu Paul K. and O. Ali, *Annals of Physics* **436**, 168722 (2022).
- [73] R. C. Pantig and A. Övgün, *Eur. Phys. J. C* **82**, 391 (2022), [arXiv:2201.03365 \[gr-qc\]](#).
- [74] A. Övgün, *Phys. Lett. B* **820**, 136517 (2021), [arXiv:2105.05035 \[gr-qc\]](#).
- [75] M. Okyay and A. Övgün, *JCAP* **01**, 009 (2022), [arXiv:2108.07766 \[gr-qc\]](#).
- [76] I. Çimdiker, D. Demir, and A. Övgün, *Phys. Dark Univ.* **34**, 100900 (2021), [arXiv:2110.11904 \[gr-qc\]](#).
- [77] R. C. Pantig and A. Övgün, (2022), [arXiv:2202.07404 \[astro-ph.GA\]](#).
- [78] X.-M. Kuang and A. Övgün, (2022), [arXiv:2205.11003 \[gr-qc\]](#).
- [79] A. Uniyal, R. C. Pantig, and A. Övgün, (2022), [arXiv:2205.11072 \[gr-qc\]](#).
- [80] A. Övgün, I. Sakallı, and J. Saavedra, *JCAP* **10**, 041 (2018), [arXiv:1807.00388 \[gr-qc\]](#).
- [81] A. Övgün and I. Sakallı, *Class. Quant. Grav.* **37**, 225003 (2020), [arXiv:2005.00982 \[gr-qc\]](#).
- [82] K. S. Virbhadra and G. F. R. Ellis, *Phys. Rev. D* **62**, 084003 (2000), [arXiv:astro-ph/9904193](#).
- [83] V. Bozza, *Phys. Rev. D* **66**, 103001 (2002), [arXiv:gr-qc/0208075](#).
- [84] W. Hasse and V. Perlick, *Gen. Rel. Grav.* **34**, 415 (2002), [arXiv:gr-qc/0108002](#).
- [85] V. Perlick, *Phys. Rev. D* **69**, 064017 (2004), [arXiv:gr-qc/0307072](#).
- [86] G. He, X. Zhou, Z. Feng, X. Mu, H. Wang, W. Li, C. Pan, and W. Lin, *Eur. Phys. J. C* **80**, 835 (2020).
- [87] G. W. Gibbons and M. C. Werner, *Class. Quant. Grav.* **25**, 235009 (2008), [arXiv:0807.0854 \[gr-qc\]](#).
- [88] M. C. Werner, *Gen. Relativ. Gravit.* **44**, 3047 (2012).
- [89] A. Övgün, *Phys. Rev. D* **98**, 044033 (2018), [arXiv:1805.06296 \[gr-qc\]](#).
- [90] A. Övgün, *Phys. Rev. D* **99**, 104075 (2019), [arXiv:1902.04411 \[gr-qc\]](#).
- [91] A. Övgün, *Universe* **5**, 115 (2019), [arXiv:1806.05549 \[physics.gen-ph\]](#).
- [92] W. Javed, J. Abbas, and A. Övgün, *Eur. Phys. J. C* **79**, 694 (2019), [arXiv:1908.09632 \[physics.gen-ph\]](#).
- [93] W. Javed, J. Abbas, and A. Övgün, *Phys. Rev. D* **100**, 044052 (2019), [arXiv:1908.05241 \[gr-qc\]](#).
- [94] W. Javed, R. Babar, and A. Övgün, *Phys. Rev. D* **100**, 104032 (2019), [arXiv:1910.11697 \[gr-qc\]](#).
- [95] W. Javed, A. Hamza, and A. Övgün, *Phys. Rev. D* **101**, 103521 (2020), [arXiv:2005.09464 \[gr-qc\]](#).
- [96] W. Javed, R. Babar, and A. Övgün, *Phys. Rev. D* **99**, 084012 (2019), [arXiv:1903.11657 \[gr-qc\]](#).
- [97] A. Övgün, I. Sakallı, and J. Saavedra, *Annals Phys.* **411**, 167978 (2019), [arXiv:1806.06453 \[gr-qc\]](#).
- [98] W. Javed, J. Abbas, and A. Övgün, *Annals Phys.* **418**, 168183 (2020), [arXiv:2007.16027 \[gr-qc\]](#).
- [99] A. Ishihara, Y. Suzuki, T. Ono, T. Kitamura, and H. Asada, *Phys. Rev. D* **94**, 084015 (2016), [arXiv:1604.08308 \[gr-qc\]](#).
- [100] K. Takizawa, T. Ono, and H. Asada, *Phys. Rev. D* **101**, 104032 (2020), [arXiv:2001.03290 \[gr-qc\]](#).
- [101] T. Ono and H. Asada, *Universe* **5**, 218 (2019), [arXiv:1906.02414 \[gr-qc\]](#).
- [102] A. Ishihara, Y. Suzuki, T. Ono, and H. Asada, *Phys. Rev. D* **95**, 044017 (2017).
- [103] T. Ono, A. Ishihara, and H. Asada, *Phys. Rev. D* **96**, 104037 (2017).
- [104] Z. Li and A. Övgün, *Phys. Rev. D* **101**, 024040 (2020).
- [105] Z. Li, G. Zhang, and A. Övgün, *Phys. Rev. D* **101**, 124058 (2020).
- [106] R. C. Pantig and E. T. Rodulfo, *Chin. J. Phys.* **66**, 691 (2020).
- [107] A. Ishihara, Y. Suzuki, T. Ono, *et al.*, *Phys. Rev. D* **94** (2016), 10.1103/physrevd.94.084015.
- [108] V. Perlick, O. Y. Tsupko, and G. S. Bisnovaty-Kogan, *Phys. Rev. D* **92**, 104031 (2015).
- [109] C. J. Gao and S. N. Zhang, *Phys. Lett. B* **595**, 28 (2004), [arXiv:gr-qc/0407045](#).
- [110] M. Jaroszynski and A. Kurpiewski, *Astron. Astrophys.* **326**, 419 (1997), [arXiv:astro-ph/9705044](#).
- [111] C. Bambi, *Astrophys. J.* **761**, 174 (2012), [arXiv:1210.5679 \[gr-qc\]](#).
- [112] P. Boonserm, T. Ngampitipan, and M. Visser, *Phys. Rev. D* **88**, 041502 (2013), [arXiv:1305.1416 \[gr-qc\]](#).
- [113] E. Berti, V. Cardoso, and A. O. Starinets, *Class. Quant. Grav.* **26**, 163001 (2009), [arXiv:0905.2975 \[gr-qc\]](#).
- [114] R. A. Konoplya and A. Zhidenko, *Rev. Mod. Phys.* **83**, 793

- (2011), [arXiv:1102.4014 \[gr-qc\]](#).
- [115] K. D. Kokkotas and B. G. Schmidt, *Living Rev. Rel.* **2**, 2 (1999), [arXiv:gr-qc/9909058](#).
- [116] V. Cardoso, A. S. Miranda, E. Berti, H. Witek, and V. T. Zanchin, *Phys. Rev. D* **79**, 064016 (2009), [arXiv:0812.1806 \[hep-th\]](#).
- [117] R. A. Konoplya and Z. Stuchlík, *Phys. Lett. B* **771**, 597 (2017), [arXiv:1705.05928 \[gr-qc\]](#).
- [118] K. Glampedakis and H. O. Silva, *Phys. Rev. D* **100**, 044040 (2019), [arXiv:1906.05455 \[gr-qc\]](#).
- [119] M. S. Churilova, *Eur. Phys. J. C* **79**, 629 (2019), [arXiv:1905.04536 \[gr-qc\]](#).
- [120] H. Kodama and A. Ishibashi, *Prog. Theor. Phys.* **110**, 701 (2003), [arXiv:hep-th/0305147](#).
- [121] M. Visser, *Phys. Rev. A* **59**, 427 (1999), [arXiv:quant-ph/9901030](#).
- [122] P. Boonserm and M. Visser, *Phys. Rev. D* **78**, 101502 (2008), [arXiv:0806.2209 \[gr-qc\]](#).
- [123] N. G. Sanchez, *Phys. Rev. D* **18**, 1030 (1978).
- [124] S. R. Das, G. W. Gibbons, and S. D. Mathur, *Phys. Rev. Lett.* **78**, 417 (1997), [arXiv:hep-th/9609052](#).
- [125] Y. Decanini, G. Esposito-Farese, and A. Folacci, *Phys. Rev. D* **83**, 044032 (2011), [arXiv:1101.0781 \[gr-qc\]](#).
- [126] R. B. Magalhães, L. C. S. Leite, and L. C. B. Crispino, *Eur. Phys. J. C* **80**, 386 (2020), [arXiv:2005.04515 \[gr-qc\]](#).
- [127] M. A. A. Paula, L. C. S. Leite, and L. C. B. Crispino, *Phys. Rev. D* **102**, 104033 (2020), [arXiv:2011.08633 \[gr-qc\]](#).
- [128] H. C. D. Lima, C. L. Benone, and L. C. B. Crispino, *Phys. Lett. B* **811**, 135921 (2020), [arXiv:2011.13446 \[gr-qc\]](#).
- [129] P. Boonserm, T. Ngampitipan, and P. Wongjun, *Eur. Phys. J. C* **79**, 330 (2019), [arXiv:1902.05215 \[gr-qc\]](#).
- [130] S. V. M. C. B. Xavier, C. L. Benone, and L. C. B. Crispino, *Eur. Phys. J. C* **81**, 1127 (2021), [arXiv:2112.12865 \[gr-qc\]](#).